

1071-36120

NASA TECHNICAL
MEMORANDUM



NASA TM X-2384

NASA TM X-2384

CASE FILE
COPY

1971 NASA TURBINE COOLING
RESEARCH STATUS REPORT

*by John N. B. Livingood, Herman H. Ellerbrock,
and Albert Kaufman*

*Lewis Research Center
Cleveland, Ohio 44135*

1. Report No. NASA TM X-2384	2. Government Accession No.	3. Recipient's Catalog No.	
4. Title and Subtitle 1971 NASA TURBINE COOLING RESEARCH STATUS REPORT		5. Report Date September 1971	6. Performing Organization Code
		8. Performing Organization Report No. E-6164	10. Work Unit No. 720-03
7. Author(s) John N. B. Livingood, Herman H. Ellerbrock, and Albert Kaufman		11. Contract or Grant No.	
9. Performing Organization Name and Address Lewis Research Center National Aeronautics and Space Administration Cleveland, Ohio 44135		13. Type of Report and Period Covered Technical Memorandum	
		14. Sponsoring Agency Code	
12. Sponsoring Agency Name and Address National Aeronautics and Space Administration Washington, D.C. 20546		15. Supplementary Notes	
16. Abstract The turbine cooling program in progress at the NASA Lewis Research Center is discussed. Research in progress at Lewis and research being performed for Lewis under contract are included. This report represents the status of work through April 1971. From comparisons of predicted and experimental results, areas requiring further research efforts are identified. Flow, heat-transfer, structure, and life considerations are presented. Cooling concepts for application to future aircraft engines are also discussed.			
17. Key Words (Suggested by Author(s)) Turbine cooling Heat transfer		18. Distribution Statement Unclassified - unlimited	
19. Security Classif. (of this report) Unclassified	20. Security Classif. (of this page) Unclassified	21. No. of Pages 83	22. Price* \$3.00

1971 NASA TURBINE COOLING RESEARCH STATUS REPORT

by John N. B. Livingood, Herman H. Ellerbrock, and Albert Kaufman

Lewis Research Center

SUMMARY

The turbine cooling program of the NASA Lewis Research Center is reviewed. This review covers work at Lewis and work being done for Lewis under contract through April 1971. The limitations of convection cooling, and the current state of the art of such cooling methods as film cooling, impingement cooling, transpiration cooling, and fuel cooling are discussed. Analytical procedures and experimental facilities currently in use are described. Cooling concepts that might be applicable to aircraft engines of the future are also presented.

Both predicted and experimental flow and heat-transfer results are presented for typical turbine vanes and blades. Predicted and experimental results are compared when possible. As a result of these comparisons, areas where further research is necessary are identified.

In addition to flow and heat-transfer research, vane and blade fabrication and structural problems are discussed, and the initial phases of blade life research currently in progress are included.

Some specific results are worthy of note. For a convection cooled vane operating at 1811 K (2800^o F) or higher, a 40-percent reduction in wall thickness (consistent with structural considerations) will yield a greater savings in coolant flow than would a 100-percent effective convection cooled vane (which, of course, is impossible to achieve). A 477 K (400^o F) reduction in coolant temperature or a 367 K (200^o F) improvement in the limiting temperature capability of the material would require the same coolant flow; each in turn requires less coolant than a 100-percent effective convection cooled vane.

As chord size is decreased on a convection cooled blade, required coolant flow, in general, increases.

A method for scaling low-gas-temperature vane heat-transfer data to high gas temperature cases was verified with high gas temperature data and proved successful. This reduces the need for extensive high gas temperature runs.

Temperature data obtained for a typical vane operated over a wide range of conditions in a static cascade correlated within 10 percent when a temperature difference ratio was plotted against the coolant to gas flow ratio.

INTRODUCTION

The NASA Lewis Research Center is engaged in a continuing program to investigate turbine cooling for application to aircraft gas turbine engines. This report (1) reviews that program, (2) indicates how and with what facilities the research is conducted, (3) presents some results that have been obtained to date, (4) discusses the potentials of various cooling methods, (5) discusses cooling concepts for future application, (6) discusses vane and blade fabrication problems, and (7) discusses research being performed to improve vane and blade life. This report represents the status of work through April 1971.

The trend in both military and commercial gas turbine engines is toward turbofan engines having compact, high temperature, high pressure gas generators or "cores." As the turbine inlet temperature is increased, it is necessary to increase the compressor pressure ratio in order to obtain minimum specific fuel consumption; therefore, increases in turbine inlet temperature will generally be accompanied by increases in the compressor pressure ratio. It seems probable that turbine inlet temperatures equivalent to those achieved by stoichiometric combustion will be employed in at least some future gas turbine engines. For JP type of fuels burning at stoichiometric fuel-air ratios, the resulting combustion gas temperature will be on the order of 2200 to 2480 K (3500^o to 4000^o F) or higher. For gas temperatures up to about 2022 K (3000^o F), the associated compressor pressure ratio may be on the order of 30 or 40 to 1; for stoichiometric gas temperatures, pressure ratios less than 30 may be used.

The NASA turbine cooling research goals are

- (1) To develop improved methods for predicting vane and blade local temperatures for all types of cooling processes
- (2) To develop methods for predicting vane and blade life
- (3) To investigate cooling concepts for future high temperature, high pressure engines
- (4) To investigate advanced metal joining techniques that can be employed to fabricate vanes and blades having high cooling effectiveness

Up to the present time convection cooling with air has been the primary means of cooling the vanes and blades of aircraft gas turbines. In some instances augmentation of the convection cooling has been achieved by the use of film cooling from holes or slots located in certain critical regions of the vane or blade airfoil. For the severe cooling conditions anticipated for future high-temperature, high-pressure engines, it is unlikely that convection cooling alone will be adequate; therefore, more effective cooling processes such as full-coverage film cooling and transpiration cooling will be required. Reference 1 discusses these various cooling methods, analyzes their limitations, and indicates their future potential in terms of turbine inlet temperature, gas pressure, and relative coolant-flow requirements. Reference 2 discusses the cooling potential of convection cooled turbines, including the effects of reduced cooling temperature, for Mach 3

flight conditions. References 3 to 11 report research that has been conducted on film and transpiration cooling; references 12 and 13 discuss impingement cooling.

Presently most convection cooled turbine vanes and blades are made from one-piece castings of nickel-base or cobalt-base high-temperature alloys. For some cooling applications, sheet metal inserts are placed within the finished castings to provide impingement cooling. In order to use some of the most effective advanced convection cooling concepts, the vanes and blades may have to be fabricated in separate subassemblies and then joined together. Two promising joining processes that might be used to bond vane and blade subcomponents together with resulting high joint efficiencies are activated diffusion brazing and gas-pressure welding. Both of these processes are discussed in reference 14.

The major Lewis Research Center experimental research facilities for turbine cooling are a static cascade facility, a modified J-75 research engine, and a flow apparatus for studies of airflow within vanes, blades, and turbine disk components. Some of the initial results obtained from these facilities as well as results obtained from contractual research are presented herein.

Experimental results from the static cascade and engine facilities cover combustion gas temperatures ranging from about 828 to 1505 K (1030^o to 2250^o F), gas pressures from 12 to 96 newtons per square centimeter (18 to 140 psia) and coolant temperatures from 297 to 756 K (75^o to 900^o F). Results from the flow facility are for air temperatures ranging from 300 to 811 K (80^o to 1000^o F) and inlet pressures from 19 to 50 newtons per square centimeter (28 to 73 psia).

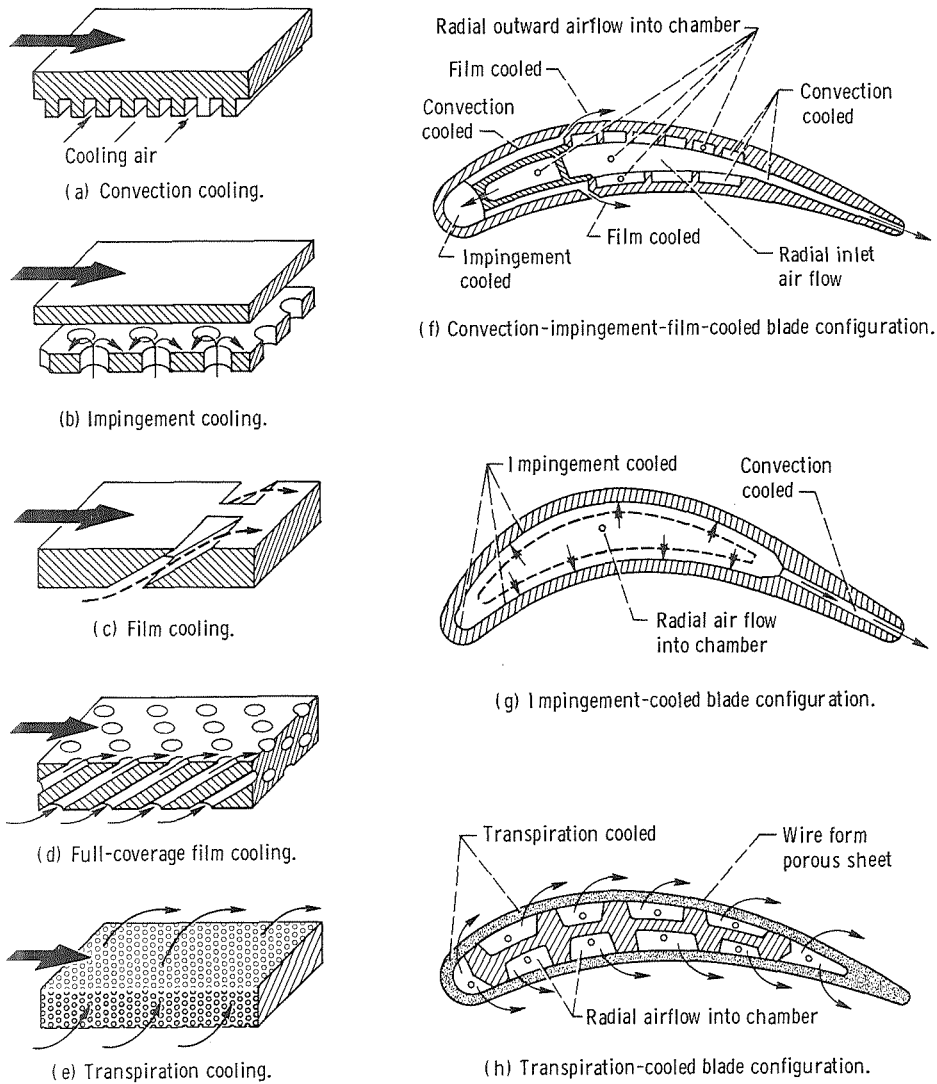
Some of the material presented herein appears in reference 15, a paper presented at the Aircraft Propulsion Conference at the Lewis Research Center on November 18-19, 1970.

Assistance in the preparation of parts of this report was given by R. P. Dengler, D. J. Gauntner, J. W. Gauntner, H. J. Gladden, J. F. Lubomski, and H. T. Richards. This assistance is greatly appreciated by the authors.

METHODS FOR TURBINE BLADE COOLING

DESCRIPTION OF COOLING METHODS

Several methods of turbine blade cooling with air as the coolant are illustrated on the left side of figure 1. The least complicated method shown is convection cooling (fig. 1(a)) where heat picked up by the blade from the hot gas is conducted through the blade wall to cooling air that is flowing through internal passages in the blade. A variation of convection cooling that can be used in certain local areas on the blade is impingement cooling



CD-11056-33

Figure 1. - Methods for turbine blade cooling.

illustrated in figure 1(b). In this method, jets of cooling air are directed against the inner surface of the blade wall to transfer heat from the metal to the coolant in a more efficient way than can be done with normal convection cooling. Even more efficient use of the cooling air can be made with film cooling by passing the air through holes or slots in the blade wall so as to establish a film of relatively cool air on the outer surface of the blade (fig. 1(c)). The cooling effect of this film dissipates quickly in the presence of the gas stream and the film must be renewed with additional holes if more than local cooling is desired. Figure 1(d) shows these additional cooling holes as full coverage film cooling. The most efficient use of cooling air can be attained with transpiration cooling by

passing the air through a porous wall to establish a complete and continuous blanket of cool air on the outer surface of the blade (fig. 1(e)).

EXAMPLES OF COOLED CONFIGURATIONS

Three typical blade configurations incorporating the various cooling methods described are also shown in figures 1(f) to (h). In figure 1(f), three of the cooling methods described above are combined. The cooling air enters the blade in several parallel radial flow paths. Air in the forwardmost flow path impinges on the inner surface of the leading edge of the blade through a radial array of holes. This air then flows chordwise toward the rear on both sides of the blade to convection cool the forward portion of the blade immediately behind the leading edge. Slots in the blade wall transfer the air to the outer surface of the blade to establish a film-cooling layer. Air in the midchord region flows radially outward in channels adjacent to the blade outer wall. This airflow makes a 180° turn at the blade tip to enter the central midchord cavity. The air then flows radially inward and discharges from the central cavity through trailing edge slots.

Figure 1(g) is an example of an all-impingement cooled blade. Cooling air enters this blade in radial flow in the central cavity and passes through holes in the insert to impinge on the inner surface of the blade wall. All cooling air then flows chordwise to the rear between the blade wall and the insert to further convection cool the blade. The cooling air exits through convection cooling slots in the trailing edge of the blade.

Figure 1(h) is a transpiration-cooled blade. A fluted support strut is the structural part of the blade. The porous material, which is the blade wall, is attached to this fluted strut. The channels formed by the flutes act as radial coolant flow passages. From these channels, the coolant passes through the porous wall, picks up heat by convection, and forms a protective film on the outer surface of the blade.

POTENTIALS OF COOLING METHODS

SIMPLIFIED COMPARISON OF COOLING METHODS

To date, convection cooling has been the primary means of cooling gas turbine engines, with some augmentation of this cooling using film cooling slots in critical regions. At the severe cooling conditions expected in future engines, it is likely that convection cooling alone will be inadequate, and more advanced cooling schemes such as full coverage film and transpiration cooling will have to be used. The potentials of convection cooling can be determined in a relatively simple manner by considering the blades as heat ex-

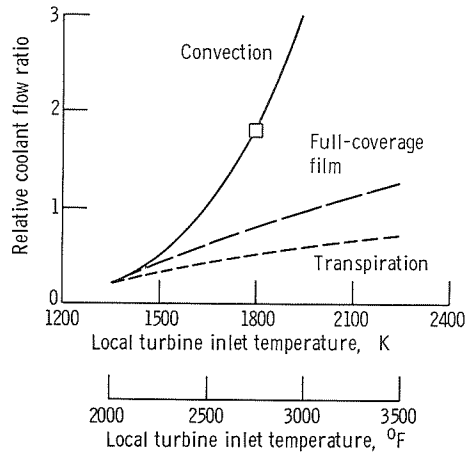


Figure 2. - Potentials of cooling methods.
 Outside metal temperature, 1255 K (1800° F);
 coolant temperature, 811 K (1000° F); wall
 thickness, 0.127 centimeter (0.05 in.); gas
 pressure, 20 atmospheres; convection effi-
 ciency, 0.7; film cooling efficiency, 0.6;
 transpiration cooling efficiency, 0.8.

changers and evaluating the cooling requirements on a basis of the heat capacity of the cooling air flowing through the blades. An example of such an evaluation is shown in figure 2 (from ref. 1) as a relationship of relative coolant flow required and turbine-inlet temperature. For this evaluation, a convection efficiency of 0.7 was assumed. Convection efficiency is defined as the ratio of the rise in cooling air temperature to the maximum potential rise in cooling air temperature. Mathematically this can be expressed as

$$\eta'_{\text{conv}} = \frac{T_{c,o} - T_{c,i}}{T_{w,i} - T_{c,i}}$$

It is further assumed that the blade temperature $T_{w,o}$ is 1255 K (1800° F), the coolant temperature $T_{c,i}$ is 811 K (1000° F), the gas stream pressure is 20 atmospheres, and the blade wall thickness is 0.127 centimeter (0.05 in.). As a basis of comparison, the coolant flow required to convectively cool the blade at a turbine inlet temperature of 1645 K (2500° F) was assigned the value of one. All other coolant flows were referenced to this basis. As can be seen in figure 2, the required coolant flow for convection cooling rises very rapidly over the range of turbine inlet temperatures considered. At 1922 K (3000° F), the required coolant flow is three times that required at 1645 K (2500° F).

Also shown in figure 2 are curves for full-coverage film and transpiration-cooled blades. The same conditions were used to develop these curves as were used for the convection curve except that the efficiency of film cooling was assumed to be 0.6 and the efficiency of transpiration cooling was assumed to be 0.8. The definitions of these efficien-

cies are the same as for the convection efficiency except that the blade outside surface temperature is substituted for the blade inside surface temperature. From figure 2 it can be seen that the required coolant flows for full-coverage film and transpiration cooling at 1645 K (2500° F) are about 60 and 40 percent of the required convection cooling respectively. When turbine inlet temperature is increased to 1922 K (3000° F), the required coolant flow increases by about 50 percent for full-coverage film and by about 40 percent for transpiration cooling. Even at 2200 K (3500° F), the required coolant flows for these two cooling methods compare favorably with the required coolant flow for convection cooling at a turbine inlet temperature of 1645 K (2500° F). Thus it can be seen that under the assigned environmental conditions, convection cooling is ineffective at the higher turbine inlet temperatures.

At temperature levels where convection cooling can provide adequate protection, however, this method does have several advantages over film and transpiration cooling. The holes or slots in the blade wall that are required for film cooling and the porous wall that is required for transpiration cooling result in structures that are inherently weaker than the solid wall of a convection-cooled blade. Also, these opening in the blade walls are susceptible to vibration and fatigue failures. Foreign-object damage and clogging of the very small coolant passages by surface oxidation or dirty cooling air can be serious problems in film or transpiration-cooled blades. Cooling air flowing through film cooling holes and porous walls may also affect aerodynamic performance. Fabrication techniques for film and transpiration-cooled blades are usually more complicated and more unconventional than the fabrication techniques for convection-cooled blades. Therefore, ways of improving convection cooling should be investigated.

POSSIBLE IMPROVEMENTS IN CONVECTION COOLING

Some possible improvements in convection cooling are shown in figure 3 (from ref. 1). These improvements are for the conditions represented by the square symbol in

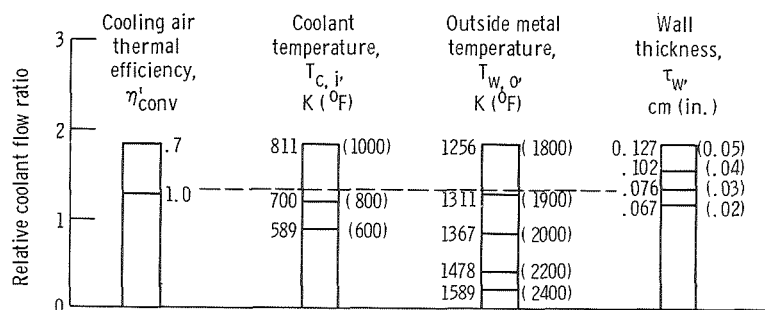


Figure 3. - Improving convection cooling. Gas temperature, 1783 K (2750° F).

figure 2. First, consider the possible improvement with increased convective efficiency. If a vane cooling configuration with an ideal, but unobtainable, 100-percent convection efficiency could be produced, the relative coolant flow ratio could be reduced as shown by the bar on the left of figure 3. Approximately the same magnitude of coolant flow reduction can be obtained by reducing the vane wall thickness from 0.127 to 0.076 centimeter (0.050 to 0.03 in.) as shown by the bar on the right of figure 3. Thinner walls result in a smaller temperature drop through the walls. For a constant outside wall surface temperature, which may be determined by oxidation limitations, a smaller temperature drop through the wall results in a larger temperature difference between the wall temperature and the cooling air temperature. This larger temperature difference permits better utilization of the cooling air by allowing higher cooling air temperature rises. It can be concluded, therefore, that for high temperature applications, the wall should be made as thin as possible consistent with structural considerations such as thin wall material properties, foreign object damage, gas pressure forces, and oxidation effects.

Even greater improvements in convection cooling can be obtained by reducing the coolant temperature or increasing the allowable vane metal temperature. The center bars in figure 3 show the effects of a reduction in cooling air temperature or an increase in the allowable vane wall temperature. Comparison of the bars in figure 3 shows reductions in cooling air temperature or increases in allowable metal temperature are far more effective in permitting either higher turbine inlet temperature or lower coolant flow rates than will ever be possible by improving the cooling efficiencies of convection cooled turbine vanes.

EXPERIMENTAL APPROACH FOR EVALUATION OF COOLED CONFIGURATIONS

Experimental evaluations were made on air-cooled configurations to verify that the criteria used in the design of these configurations were valid. To provide accurate inputs for checking the design calculations, the temperature, pressure, and flow rate of both the gas stream and the cooling air are measured in the experimental testing. The design criteria can then be modified and refined on the basis of experimental results. The improved design criteria could then be used to produce better configurations. Ideally, these well-designed configurations would not have to be subjected to expensive developmental testing to determine unknown effects that were not accounted for in the design. Typical procedures for determining cooling air, gas stream, and metal temperature conditions experimentally are illustrated below.

COOLING AIRFLOW DISTRIBUTION STUDIES

On the cooling air side, the distribution of the cooling air in the various passages

within the configuration is very important. This flow distribution can be determined from airflow studies on the actual configuration. Such a study on a typical air-cooled vane configuration is described in the following paragraphs.

Description of Typical Air-Cooled Vane

The typical vane configuration referred to is shown in figure 4 and incorporates several convective cooling techniques as well as localized film cooling to achieve an effective cooling design. Vanes of this particular configuration were obtained from a vendor in private industry and were designed for operation in a gas environment of 1645 K (2500° F). Based on a coolant temperature of 672 K (750° F), the design coolant flow rate was 3.5 percent of the total gas flow rate.

Cooling air entering this vane flows into a plenum within the hollow tip platform. From here, a portion of this cooling air is directed into a radial tube in the leading-edge

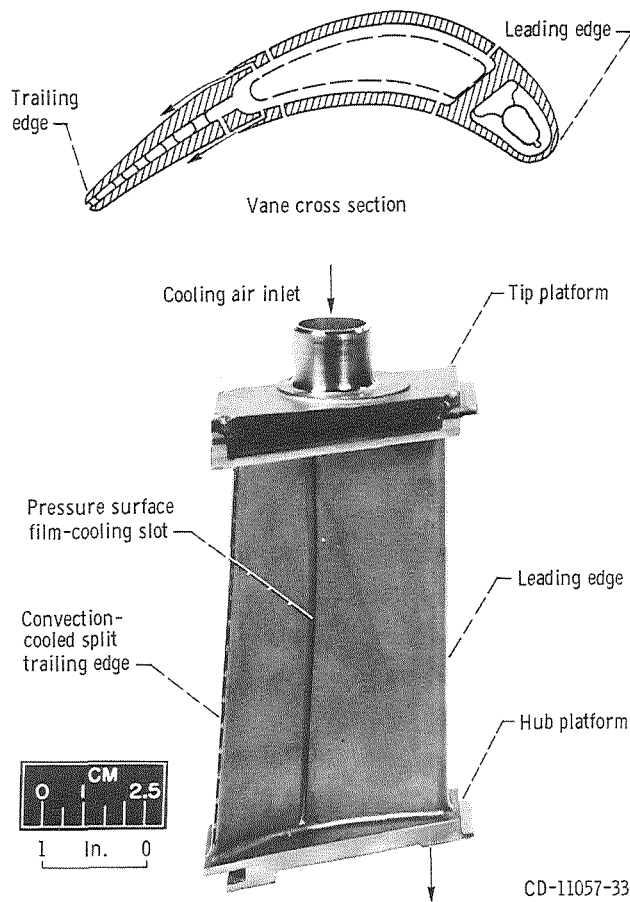


Figure 4. - Air-cooled turbine vane.

region. Air from this tube then flows through slots in the tube to impinge on the vane leading edge to effectively cool this region. Continuing on, this air then splits up and flows rearward in a chordwise direction through finned passages on both the pressure and suction sides of the vane and eventually exits beneath the vane hub platform from a radial cavity. The remaining portion of cooling air entering the vane is directed from the tip platform plenum to a cavity in the vane midchord region. From here the air flows through an array of small holes in a pair of sheet metal inserts to impinge and cool the internal sides of both the pressure and suction surfaces of the vane. After impinging on the respective surfaces, the air flows toward the rear from both sides to meet in a common plenum from which the air further splits into three paths. Some of the air exits through radial slots in the vane pressure surface to provide a film of cooling air for the remaining portion of the vane pressure surface to the trailing edge. Some of the air also flows through radial slots in the vane suction surface to provide film cooling for the remaining vane suction surface in the trailing edge region. The other path for the remaining cooling airflow is provided by a split trailing edge. The split trailing edge passage incorporates a large number of structural pin fins which also act as turbulators and provide additional heat transfer surface.

In fabricating the small numbers of vanes and blades of each test configuration required for research purposes, techniques such as brazing, electron beam welding (EBW), and electric discharge machining (EDM) or electro-chemical machining (ECM) were used. Extensive use of these machining and joining techniques made it possible to incorporate very intricate cooling geometries without requiring a long development program. In general, fabrication of vanes and blades was achieved by first machining cooling geometries into integral base-airfoil blade halves - the parting line being along the leading and trailing edges. Sheet metal components were added (through brazing cycles) to complete various cooling passages, and finally the suction surface and pressure surface base-airfoil blade halves were joined together by electron beam welding. It should be emphasized, however, that the fabrication techniques used are not necessarily those that would be recommended for production hardware. More discussion on this will be given later.

The basic material used in fabricating these research vanes and blades was Udimet 700. This choice was dictated by the relative ease of machining and joining this material compared with other high-temperature, high-strength materials. In addition, extended blade life was not a requirement because the tests proposed for heat-transfer research purposes were of short duration.

Tests were conducted with the vane illustrated (fig. 4) in a stationary test rig (non-rotating) to determine the cooling airflow distribution and pressure changes within the vane. Heat-transfer tests in both static and rotating test rigs have also been conducted on the illustrated vane. The facilities used to obtain data for this and other test vane configurations will now be discussed.

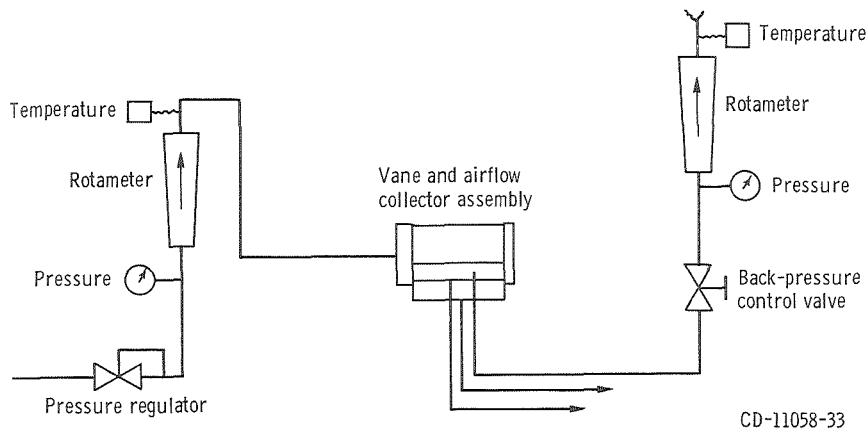
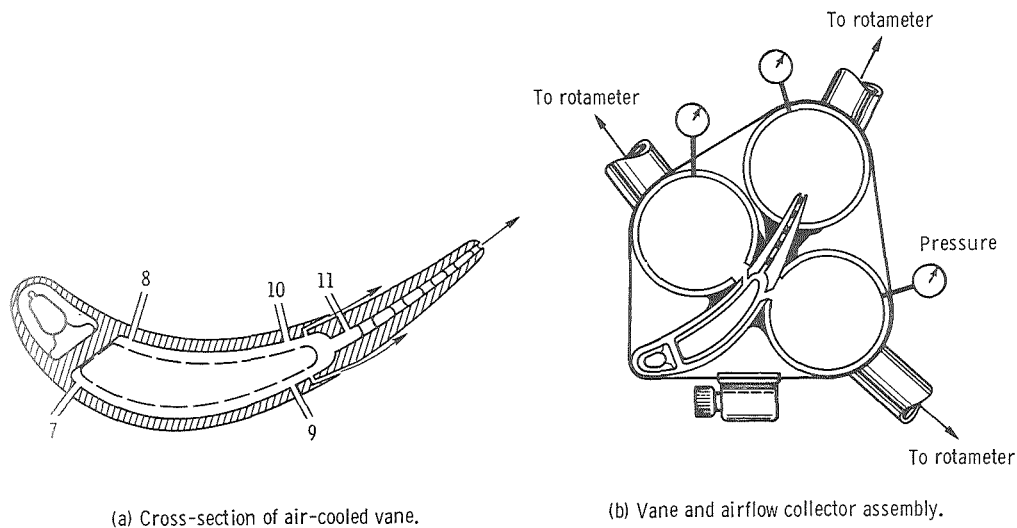
Airflow Distribution Test Apparatus

In order to study the heat transfer characteristics of cooled turbine vanes and blades, a detailed knowledge of the flow distribution and pressure changes as the coolant flows through the internal cooling passages is required. Such detailed flow measurements cannot be made during heat-transfer tests on an engine because of space limitations for instrumentation leads. Therefore, it is necessary to instrument the vanes and flow test them in a separate flow distribution apparatus in order to obtain the required experimental flow characteristics. An example of the testing of a vane and the apparatus used is given in the following discussion of figure 5.

In order to determine the flow distribution in the various parts of the vane, both flow measurements and pressure measurements were made. Static pressure taps were installed at the hub, midspan, and tip sections on the vane as illustrated in figure 5(a). Those at stations 7 and 8 were located within 0.25 centimeter (0.10 in.) of the leading edge end of the suction and pressure side flow passages. Those at stations 9 and 10 were located within 0.38 centimeter (0.15 in.) of the entrance to the metering slots that feed the suction and pressure film cooling slots. Those at station 11 were located within 0.25 centimeter (0.10 in.) of the entrance to the split trailing edge. Several other pressure measurements were made in the leading edge flow passages and in the flow collectors to be discussed. Details of these installations are available in reference 16. All pressures measured were estimated to be accurate to within ± 0.034 newtons per square centimeter (0.05 psi).

The flow that entered the vane tip through a supply tube exited through four openings. In order to measure the amount of flow exiting through each of the openings, four flow collectors were fastened to the vane at the following locations: one at the vane base leading edge region, one covering each of the two film cooling slots, and one surrounding the split trailing edge. The arrangement of the trailing edge flow collectors is shown in figure 5(b). The leading edge cooling air collector was a 1.27-centimeter (0.5-in.) diameter stainless steel tube which was welded in place to cover the discharge passage in the vane base. The other three collectors were closed-end steel cylinders with a contoured slot. For ambient tests, these cylinders were attached with an air-curing silicone sealant. Band clamps provided the necessary support for the three collecting tanks to resist the internal pressure. Air from each of these collectors exited through 1.27-centimeter (0.5-in.) diameter tubing.

The system described was satisfactory for testing at ambient temperature. However, even with the addition of a high temperature sealant, which was continuous-use rated at 589 K (600° F), the three collectors could not be sealed with the vane assembly raised to 367 K (200° F) or higher. For tests at temperatures above ambient, therefore, only the leading edge collector could be used.



(c) Schematic diagram of airflow distribution test apparatus.

Figure 5. - Airflow distribution test apparatus.

Rotameters were installed in the inlet supply piping and downstream of each of the collectors. The rotameters used were commercial models calibrated for air at densities corresponding to those expected during operation. The accuracy to be expected from these meters was 0.5 percent of full scale. For elevated air temperature tests, the heated air was cooled to room temperature before being passed through the rotameters.

The instrumented vane assembly was installed in a flow distribution apparatus shown schematically in figure 5(c). Laboratory service air at 96 newtons per square centimeter (125 psig) was dried, filtered, and passed through two successive pressure regulators to a rotameter calibrated for inlet weight flow measurement. The air was then directed through a triple-pass 25-kilowatt electric heater. The heater could be manually or automatically controlled to provide air temperatures up to 811 K (1000⁰ F) for flow rates be-

tween 4.54 and 45.4 grams per second (0.01 and 0.1 lbm/sec). The vane was attached as near to this heater as was practical with well-insulated piping.

The air from the vane leading edge exit passage was ducted to the air cooler and from this point through a throttling valve to a rotameter and then discharged to atmospheric pressure. This permitted controlling back pressure on the leading edge exit passage. Air that exited through the trailing edge passages entered a hot-air collector and was discharged to the atmosphere outside the test cell.

Ambient air tests were also run with the same apparatus with the electric heater bypassed. For these tests, flow entered the four collectors and the weight flow from each collector was measured by a rotameter.

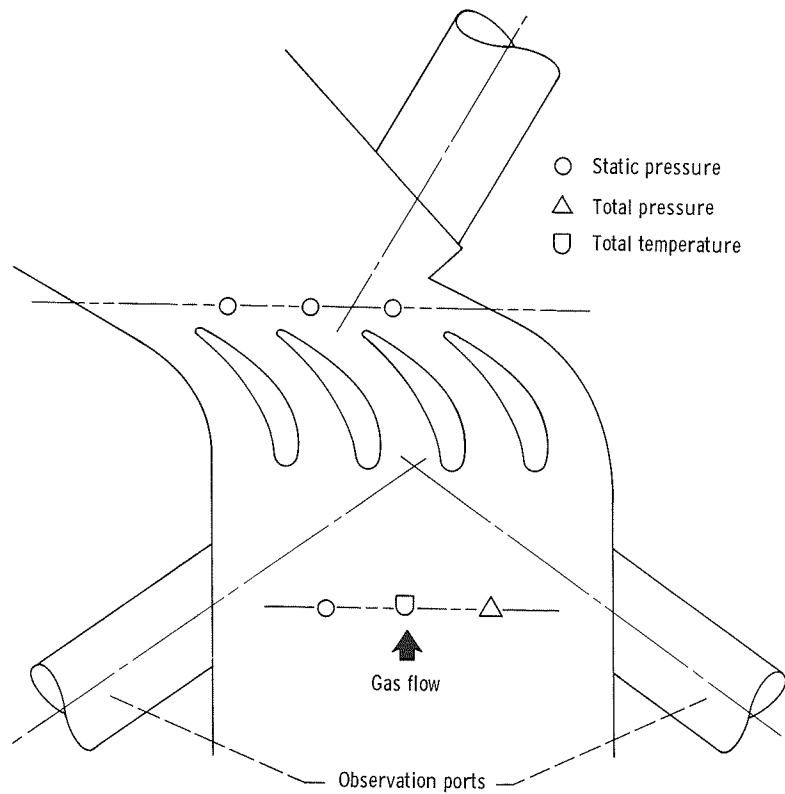
STATIC-CASCADE TESTING

Heat-transfer tests were conducted for the vane shown in figure 4 in a static cascade. The vane test section is shown in a plan view in figure 6(a). A photograph of the installed vane pack is shown in figure 6(b). The cascade was designed for continuous operation at an average inlet gas temperature of 1645 K (2500^o F) and at pressures up to 103 newtons per square centimeter (150 psia). This cascade is capable of operating at an average temperature of 1922 K (3000^o F) for short periods of time.

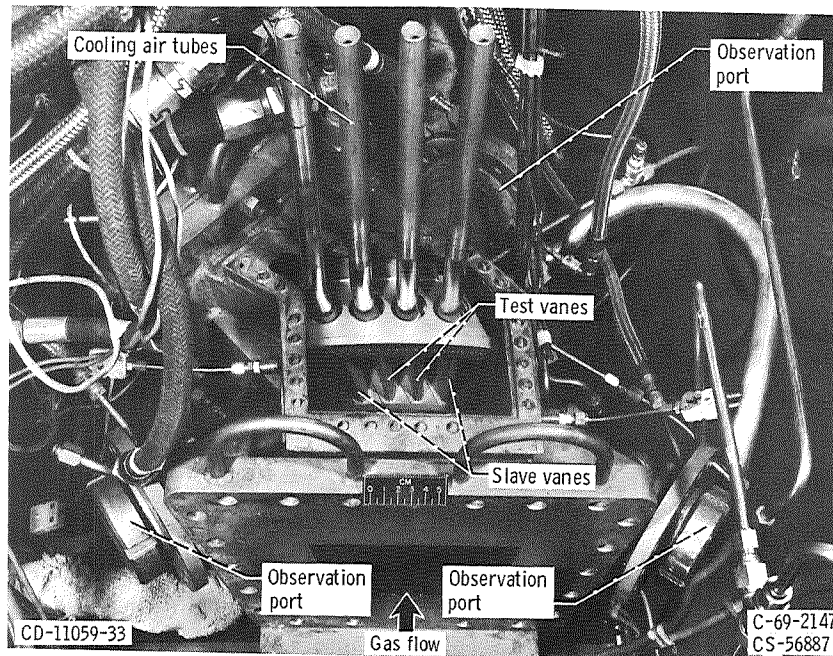
As shown in figure 6(a), the test section contains four vanes. The central two vanes are used to collect test data, and the outer two vanes are used to provide flow channels for the test vanes and to act as radiation shields between the test vanes and the water-cooled walls.

Cooling air is supplied to the vanes through three independently metered systems. One system is used to supply cooling air to the two central vanes and the other systems are used to supply cooling air to each of the outer vanes. The cooling air to the central vanes can be preheated to approximately 1033 K (1400^o F) to represent compressor bleed air. The cascade facility and associated hardware and the instrumentation and recording systems are described in more detail in reference 17.

The instrumentation for the cascade is separated into two parts: general operation instrumentation and research instrumentation. The operational instrumentation consists of those sensors required to measure quantities such as fuel flow rate, fuel pressures and temperatures, cooling water flow rates, cooling water pressures and temperatures, etc. Most of this instrumentation is connected to visual readouts in the control room. The research instrumentation consists of traversing probes upstream of the vane row to measure inlet total pressures and temperatures, static wall pressure taps upstream and downstream of the vane row, internal pressure taps and surface thermocouples on the test vanes, and various fuel, cooling air, and combustion airflow metering devices. Also



(a) Plan view



(b) Vane pack installed in cascade.

Figure 6. - Static cascade.

included for research purposes are three viewing ports, which are used for optical thermometry. A system has been developed for use with the cascade which involves a photographic procedure using commercially available infrared film and a calibrating procedure which uses a reference thermocouple. This method is described more fully in reference 18. A typical isotherm map is shown on the right side of figure 7. Located on the map are the positions of the reference thermocouple and a row of film cooling holes.

This cascade was designed primarily for heat-transfer studies; however, it is desirable to know the aerodynamic characteristics of the cascade and how they compare with a

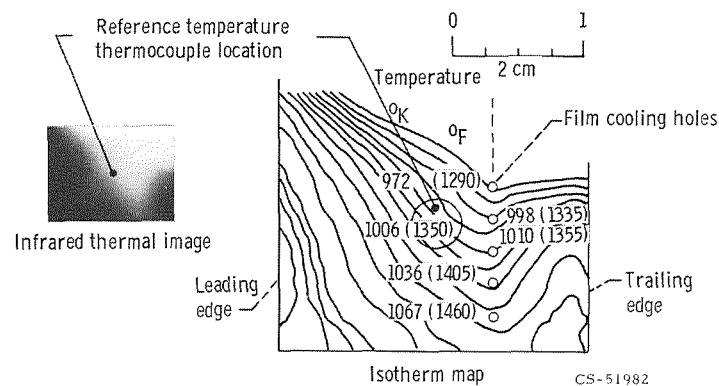


Figure 7. - Temperature measurement by infrared photography.

full annular vane row. The velocity distribution around the test vanes can be seriously affected by the cascade end wall, and this in turn will affect the calculation of gas side heat-transfer coefficients. The aerodynamic characteristics of this cascade are discussed in reference 19. The investigation reported in reference 19 considered flow around solid vanes only and did not consider secondary-flow ejection to the main air-stream (secondary flow can consist of air ejected through slots or holes, air ejected through a split trailing edge, air ejected uniformly over the vane surface (such as a porous surface), or a combination of these types of flow). Secondary-air ejection can affect the performance of a vane row. An analytical investigation of the effect of secondary flow on turbine performance is discussed in references 20 and 21. An experimental investigation of this problem is discussed in references 22, 23, and 24.

RESEARCH ENGINE TESTING

A test-bed turbojet research engine shown schematically in figure 8 is used in the Lewis turbine cooling research program to provide an engine environment for the exper-

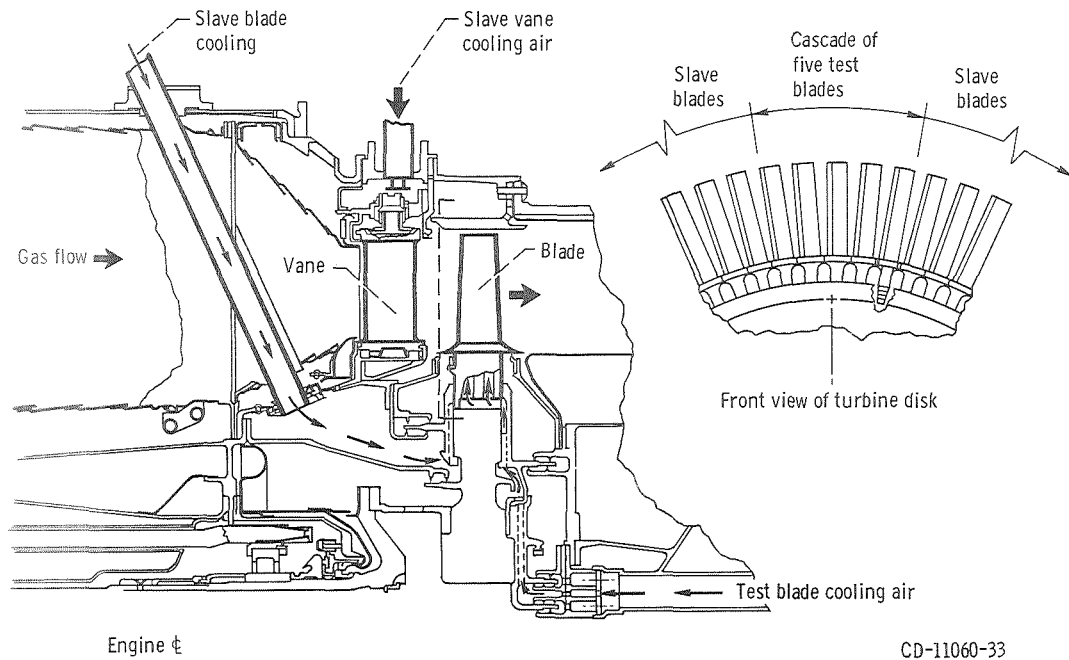


Figure 8. - Turbine cooling research engine.

imental evaluation of vane and blade configurations. This engine can be operated at turbine inlet temperatures up to 1645 K (2500^o F) and pressure levels to about 3 atmospheres. The turbine rotor contains a cascade of five test blades. This test cascade is cooled by an airflow that can be controlled in temperature and flow rate independently of the airflow for the remaining slave blades in the rotor. A balanced-pressure labyrinth seal is used on the engine to minimize leakage of test blade cooling air at the stationary-to-rotating transfer point near the engine centerline. In reference 25, an experimental leakage flow study of such a seal is presented. A combination experimental and analytical study of the entire test blade cooling airflow path from the engine centerline through the blades is presented in reference 26. With an independent cooling system for the test cascade, the determination of cooling airflow is more accurate and the slave blades can be continuously cooled with a conservative coolant flow rate at a conservative cooling air temperature while the test blades are being evaluated over ranges of coolant flow rates and temperatures. A similar test cascade of five vanes and a dual cooling air system for test vanes and slave vanes is used also in the vane row.

Temperatures on the blade and vane surfaces are measured with thermocouples. Currently, the thermocouple signals from the rotating blades are transferred to stationary read-out equipment through a slip-ring. Development work is now in progress on a rotating shaft-mounted microelectronics data system which will accomplish this signal transfer with a rotary transformer. This data system is discussed in reference 27. A

rotating carrier package with 10 pressure transducers is also being developed to make rotating pressure measurements on the blades. Signals from the transducer outputs will also be fed through the shaft data system. A more extensive description of the research engine is presented in reference 17.

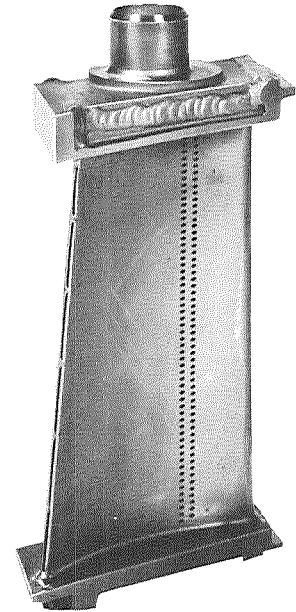
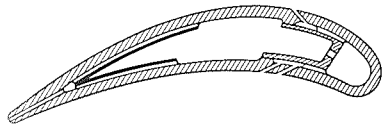
At the pressure levels for which this engine operates, heat fluxes are low compared with those in present advanced engines and in future engines. High heat fluxes cause large wall temperature gradients and create cooling problems, particularly with convection cooling as discussed in reference 1. Plans are under way for the construction of a new turbine facility that will operate at pressures up to 414 newtons per square centimeter (600 psi) and gas temperatures up to 2480 K (4000^o F) to investigate the problems of cooling future turbines. It is planned to have an external source of high pressure air for the turbine facility, and the turbine power will be absorbed by water brakes.

COOLING CONCEPTS FOR FUTURE APPLICATION

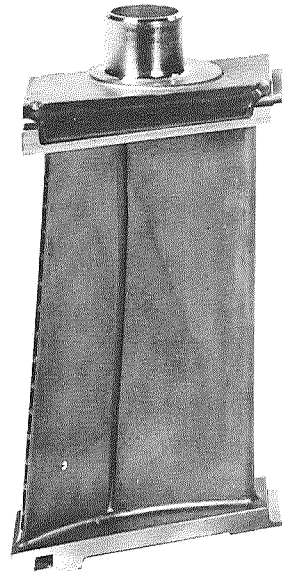
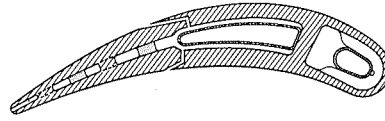
A detailed description of a typical air cooled vane currently under investigation has been given. This vane (fig. 4) incorporates film, impingement, and convection cooling. To obtain the cooling performance that will be required for the higher temperature environments of future engines, more sophisticated internal configurations will be required. This will probably mean more finning of smaller thicknesses and closer spacing for convection cooled configurations, perforated inserts to direct the jets to the proper places for impingement cooled configurations, and new ideas for supporting the walls of full-coverage film and transpiration cooled configurations. These requirements will necessitate studies of vane and blade configurations for both heat-transfer and structural characteristics. The following sections describe some of the probable cooling configurations that are proposed for use in vanes for advanced engines.

FILM-CONVECTION COOLED VANE

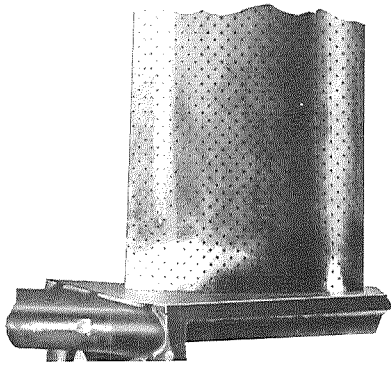
The vane shown in figure 9(a) is cooled by a combination of film and convection flows with impingement augmentation in the leading edge. Cooling air enters the midchord cavity of the vane as radial flow from the inlet air tube. Some of this air passes through a radial array of holes to impinge on the inside surface of the leading edge. This air then flows along the inside surface on both sides of the vane to be discharged into the gas stream through film cooling holes. The remainder of the cooling air in the midchord cavity enters parallel chordwise passages on both sides of the vane and flows toward the trailing edge. These passages are formed by adding thin sheet metal covers to the tops of



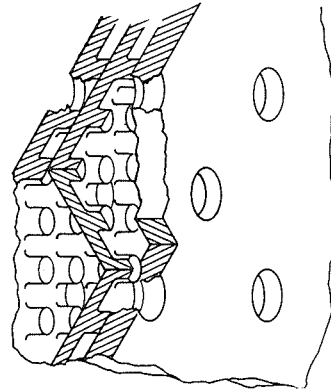
(a) Film-convection cooling.



(b) Film-impingement cooling.

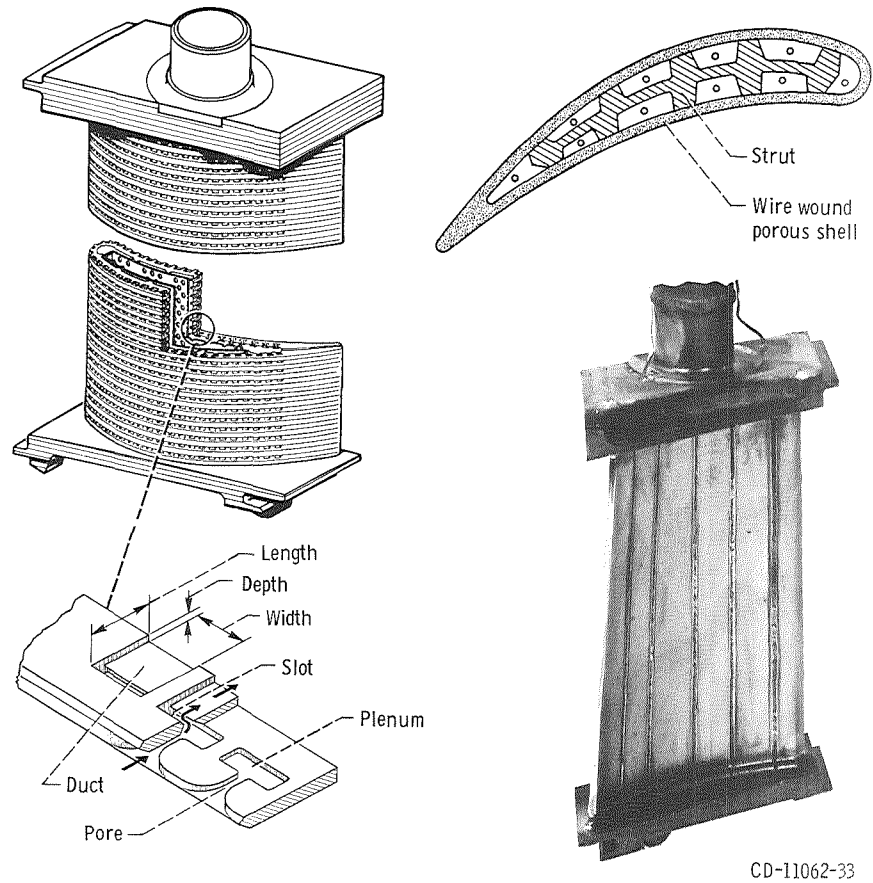


(c) Full-coverage film cooling (laminated sheet metal).



CD-11061-33

Figure 9. - Advanced cooling concepts.



(d) Full-coverage film cooling (laminated platelets).

(e) Transpiration cooling.

Figure 9. - Concluded.

an array of parallel fins machined into the vane wall. The sheet metal covers confine the airflow to convective cooling in the chordwise passages. All of this air exits through a split trailing edge to convectively cool this part of the vane.

FILM-IMPINGEMENT COOLED VANE

The vane shown in figure 9(b) is film-cooled in the trailing edge section and impingement cooled in the leading edge and midchord sections. This cooling is augmented by convection cooling in the split trailing edge and in the midchord where the air from the impingement jets exits toward the trailing edge. This is the same vane shown in figure 4; this vane configuration is also used as the slave vane in the cascade (fig. 6) and the research engine (fig. 8). The vane was made from a one-piece casting with a slotted tube in the leading edge and a perforated insert in the midchord to provide impingement cooling

in these areas. Pin fins were cast in the split trailing edge to improve the convection cooling of this region. The film cooling slots were made by EDM.

FULL-COVERAGE FILM COOLED VANES

Two types of full-coverage film cooled vanes are considered. One is constructed from laminated sheet metal and the other from laminated platelets. The number of film cooling ejection holes can be controlled in the fabrication of either type, thus assuring full coverage. High convective cooling efficiency is also obtained because of the heat pickup by the cooling air as it passes through the film cooling passages in the vane wall; the greater the number of film cooling passages, the more effective is this convection cooling.

Laminated Sheet Metal Vane

The vane shown in figure 9(c) is a full-coverage film cooled vane made of laminated sheet metal (Lamilloy). Coolant passages are photoetched in the individual laminates before bonding to form flat sheet stock. The laminated sheet is then die-formed into an air-foil contour. The size and spacings of the holes (fig. 9(c)) can be varied freely to distribute the cooling airflow as required. The hole sizes on the vane vary from 0.036 to 0.058 centimeter (0.0145 to 0.023 in.) in diameter. The hole spacings are 0.173 to 0.224 centimeter (0.068 to 0.096 in.).

The Detroit Diesel-Allison Division of the General Motors Corporation is investigating this type of material and the fabrication of vanes from this material under contract NAS 3-7913. Results of these contractual studies are presented in references 28 and 29. Based on flow, oxidation, and strength tests of this material, the contractor designed, fabricated, and tested a vane. Discussion of results of these experimental studies will be presented later.

Laminated Platelet Vane

The vane shown in figure 9(d) is another full-coverage film cooled vane made from a large number of 0.025-centimeter (0.010-in.) thick metal platelets which are diffusion bonded together. The outer periphery of each platelet is shaped to the contour of the air-foil profile. The center of each platelet is cut out to provide a central cooling air cavity. Each platelet is photoetched to provide cooling passages from the central cavity to the outer wall of the vane. These platelets are of two types that are placed alternately in the

assembly. Mating passages from two adjacent platelets are required to complete the flow path. (See the inset in fig. 9(d).) Each photoetched coolant passage in the upper platelet (shown in the inset in fig. 9(d)) consists of a slot through the platelet (in line with the plenum chamber in the lower platelet) and a relatively wide duct connecting this slot to the outer surface of the vane. The photoetched coolant passage in the lower platelet consists of a bell-mouth inlet, a pore (the size of which determines the coolant passage flow rate), and a plenum. The slot in the upper platelet and the plenum in the lower platelet are aligned to form a continuous flow path. Cooling air flowing through the combination of coolant passages in the two adjacent platelets film cools the outer wall of the vane. The multiplicity of passages provides for full-coverage film cooling. Convection cooling of the vane wall also occurs along the flow path through the platelets. In the vane shown on the left of figure 9(d), all of the vane outer surface except the extreme trailing edge region is cooled by full-coverage film cooling. The trailing edge is convectively cooled by air that is ducted through long photoetched passages in the platelets that connect the central cavity with the trailing edge.

Laminated platelet material is being made under contract NAS 3-10495 by Aerojet Liquid Rocket Company. Results of the investigation are presented in reference 30. This investigation covered a study of the flow characteristics through the small photoetched passages, the effects of oxidation on the coolant flow for platelets made from TD nickel chromium, and the strength of a diffusion bonded TD nickel chromium platelet assembly at a metal temperature of 1225 K (1800° F). From data obtained in this investigation, a full coverage film cooled vane was designed and fabricated. Five vanes are available for testing in the cascade shown in figure 6.

TRANSPIRATION COOLED VANE

A transpiration cooled vane is shown in figure 9(e). The outer shell of the vane is made by winding a flattened wire around a mandrel, removing the mandrel, splitting the wire-form tube, sintering and rolling to obtain the desired permeability. The porous shell is electron beam welded to a strut to form the vane airfoil contour. The strut supports the porous wall and also divides the central part of the vane into separate cooling air chambers. Cooling airflow into each chamber is controlled by a properly sized orifice. The cooling air flows from the chambers through the porous wall to cool the vane.

Transpiration cooling has been under investigation for some time. Curtiss-Wright has built and successfully operated transpiration cooled turbines. Results of some of the Curtiss-Wright tests are published in references 31 to 33.

TYPICAL FLOW AND HEAT TRANSFER RESULTS

As a result of research both at Lewis and by contractors, flow and heat transfer knowledge is being accumulated. Some typical examples of results being obtained will now be given for the different types of vane cooling configurations previously discussed.

COOLANT FLOW RESEARCH

Trailing Edge Friction Factors

Friction factors for staggered tube arrangements were studied by Kays and London (ref. 34) and were used to compare with experimental friction factors determined for the trailing edge of the vane shown in figure 4. A cross-sectional view of the vane trailing edge showing the staggered pin fin arrangement appears in figure 10. The friction factors are shown in figure 11. The Reynolds number (abscissa) in figure 11 is based on the hydraulic diameter of the minimum flow area in the finned trailing edge. From these results, and from other attempts to correlate flow data for other parts of the vane, as illustrated in reference 16, more detailed flow studies must be made in full-size or over-size models before a complete understanding of the vane flow characteristics is possible.

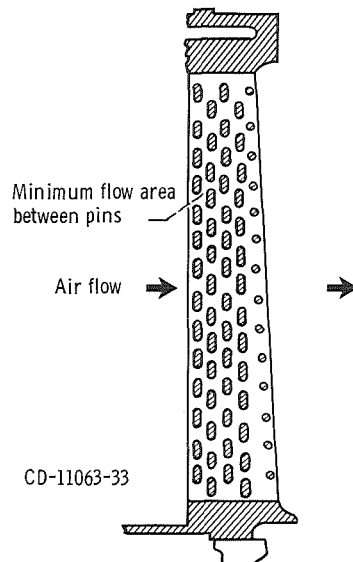


Figure 10. - Cross-sectional view of split trailing edge of vane of figure 4.

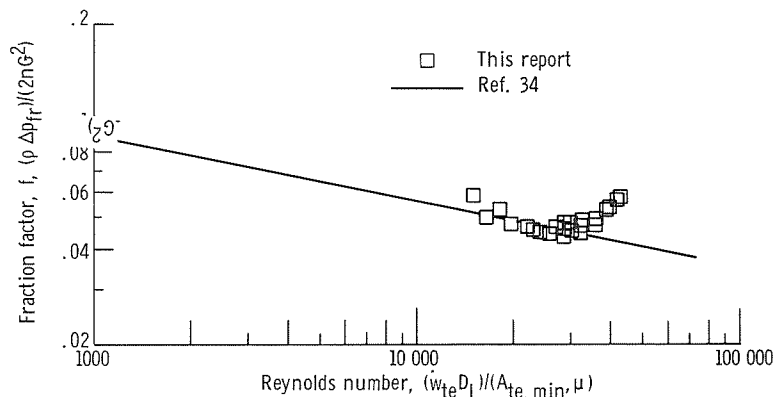


Figure 11. - Trailing-edge friction factor as function of Reynolds number.

Flow Studies in Models

The initial detailed investigation of some of the flow characteristics were made at Lewis Research Center and are reported in reference 35. This reference reports experimental discharge coefficients obtained for thick plate orifices with the approaching flow perpendicular or inclined to the orifice axis are dependent on the approach Mach number, static pressure differential across the orifice, inlet edge radius of the orifice, angle between the main flow and the orifice axis, and the ratio of the orifice thickness to diameter.

Other detailed flow studies are now being made for Lewis Research Center by the General Electric Company under contract NAS 3-13499 in both full-size and five-times-size models. The models shown in figure 12 represent the leading edge, midchord, and trailing edge regions of the vane shown in figure 4. Leading edge impingement tests will be made for several impingement spacing to nozzle diameter ratios and several flow splits. For cross flow impingement, several plate spacings, several impingement hole spacings and several rates of approach flow will be considered. Pin fin tests for several pin spacings and several plate spacings are included. Finally, a composite model incorporating each of the above three types of cooling will be built and tested.

Impingement Cooling Flow Studies

Impingement cooling heat-transfer correlations were usually obtained by use of the jet velocity through the impingement nozzle. In reality, impingement cooling heat-transfer correlations should be based on the jet velocity at local points on the impingement surface. As a consequence, an experimental study of the flow characteristics of a

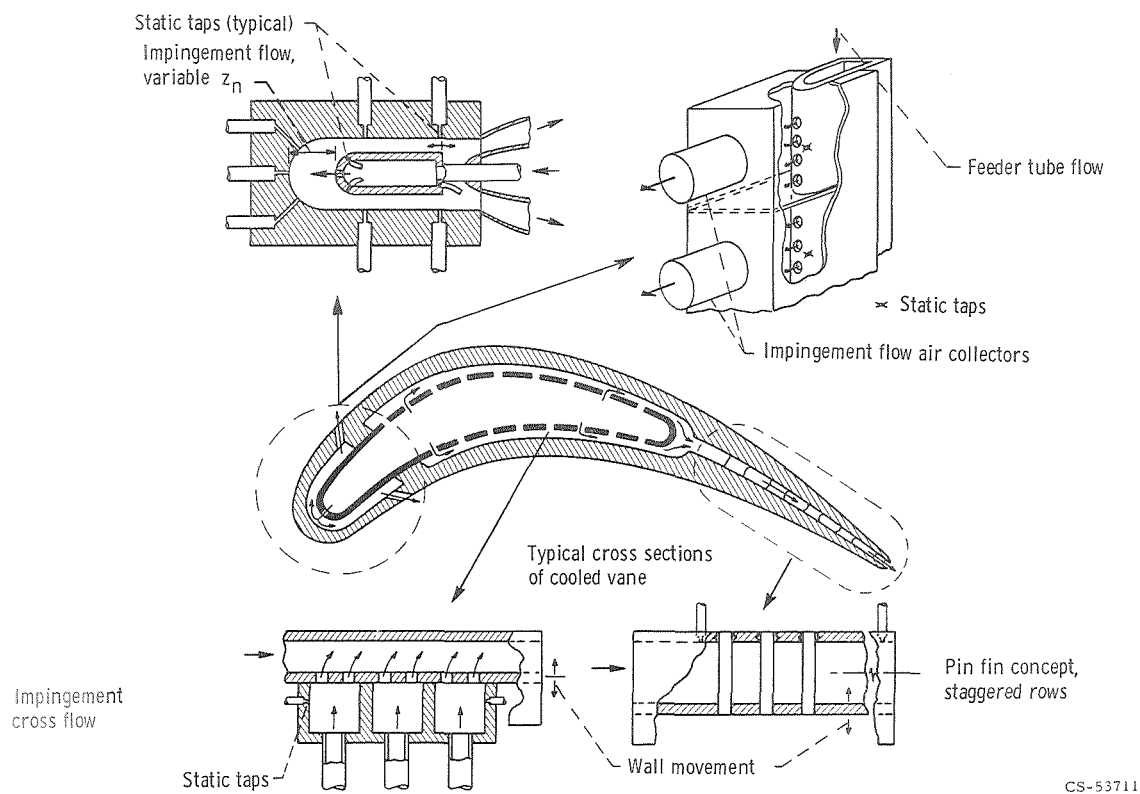


Figure 12. - Examples of models for use in detailed coolant flow studies.

jet impinging on a flat plate was made and is reported in reference 12. Information obtained from this study can probably be applied to cross-flow impingement on the suction and pressure surfaces of turbine vanes and blades.

The various flow regions formed by a jet impinging on a solid surface are shown in figure 13(a). Region I is the region of flow establishment and extends from the nozzle exit to the apex of a potential core which is formed. The potential core is the central portion of the flow in which the velocity remains constant and equal to the velocity at the nozzle exit. Region II is a region of established flow in the direction of the jet beyond the apex of the potential core; it is characterized by a dissipation of the centerline jet velocity and by a spreading of the jet in the transverse direction. Region III is that region in which the jet is deflected from the axial direction. Region IV is known as the wall jet region, where the directed flow increases in thickness as the boundary layer builds up along the solid surface.

The flow characteristics were studied in order to determine whether either new or existing laws would permit calculation of flow velocities along the plate which would agree with experimentally determined velocities. Such laws could then be applied to formulate heat-transfer correlations using these calculated velocities. An example of the flow re-

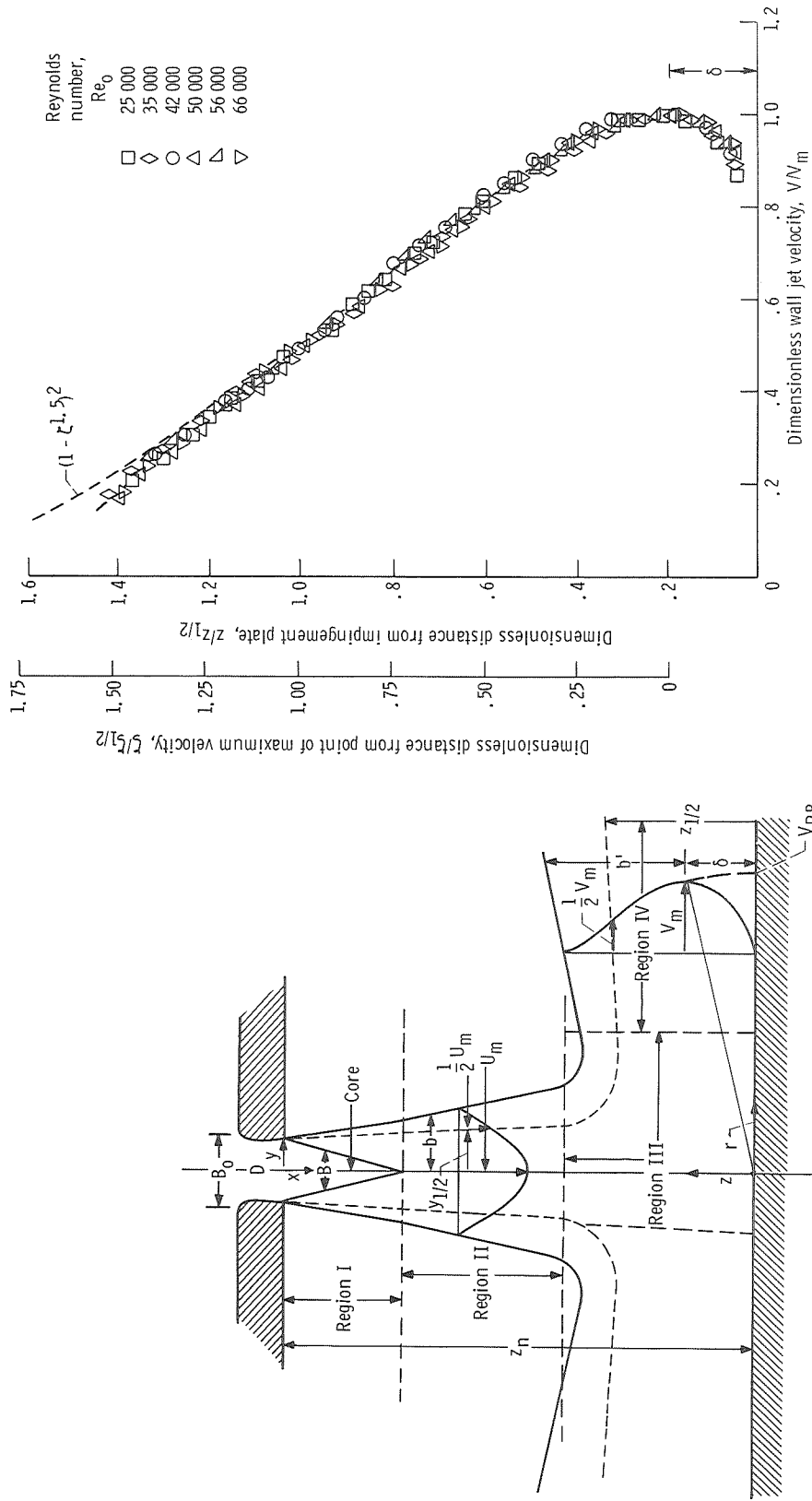


Figure 13. - Flow regions for an impinging jet and wall jet velocity profile. Distance from stagnation point, 5.08 centimeters (2 in.); nozzle diameter, 0.635 centimeters (0.25 in.); nozzle to plate spacing, 10-diameters.

sults for region IV will be discussed. Flow characteristics in all the regions are given in reference 12.

In region IV, static pressure measurements were made along the impingement plate and velocity profiles through the wall jet were determined. Figure 13(b) illustrates the velocity profile through the wall jet (region IV). The velocity increases from 0 at the plate to a maximum value V_m at a distance δ from the plate (δ is the boundary layer thickness). The velocity then decreases, reaching 1 percent at b' (the distance from the edge of the boundary layer to the edge of the wall jet).

Figure 13(b) shows the experimentally determined values of the dimensionless wall jet velocity V/V_m (V is the wall jet velocity at any position and V_m the maximum) for a range of Reynolds numbers based on nozzle velocity. The profiles are for a plate spaced 10 nozzle diameters from the nozzle and are at 5.08 centimeters (2 in.) from the stagnation point. The figure contains two ordinates. One is $z/z_{1/2}$ where z is the distance from the plate and $z_{1/2}$ is the value of z for which $V = 1/2 V_m$. The other ordinate is $\zeta/\zeta_{1/2}$ where $\zeta = z - \delta/b'$ and $\zeta_{1/2}$ is the value of ζ when z is replaced by $z_{1/2}$. The two ordinates are required in order to compare the experimental data with theoretically determined wall jet velocity distributions.

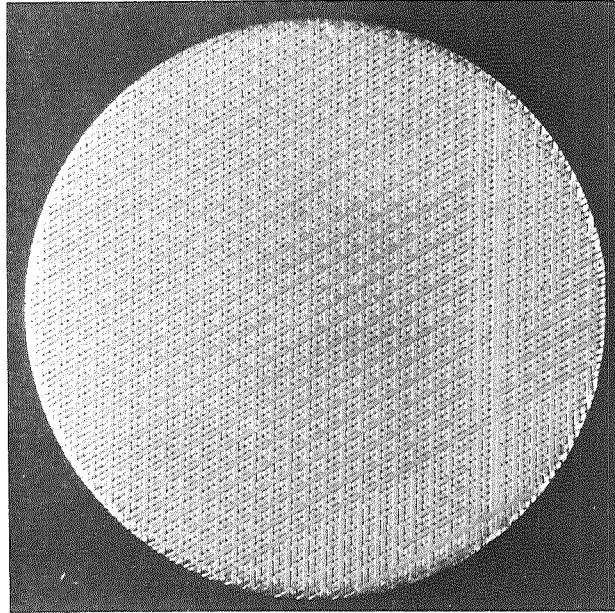
One theoretical distribution is due to Glauert (ref. 36). He divided the wall jet into an inner layer influenced by the plate and an outer layer characterized by the features of a free turbulent jet. He matched the two solutions at the boundary between the two layers (zero shear stress). Glauert's solution is not represented on figure 13(b), but the data shown in figure 13(b) have revealed that the experimental profile is lower than Glauert's in the outer portion of the jet and flatter than Glauert's at the tip. Abramovich's solution (ref. 37) is given by

$$\frac{V}{V_m} = (1 - \zeta^{3/2})^2$$

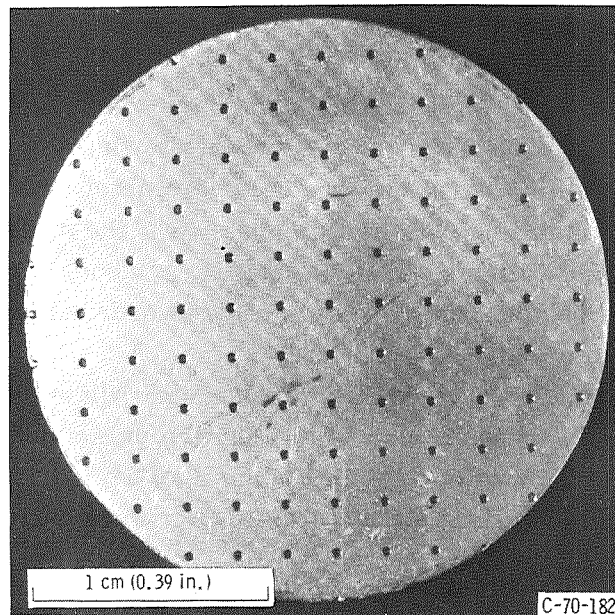
and is only valid outside the boundary layer, hence, the necessity for the second ordinate. The data agree well with the solution of Abramovich for values of $\zeta/\zeta_{1/2}$ from 0 to about 1.5, as shown in figure 13(b). It appears reasonable that the velocity at the edge of the boundary layer V_m should be used in attempts to correlate heat-transfer data in the wall jet region.

Transpiration Cooling

A knowledge of the flow characteristics for transpiration material is required in order to design vanes. Flow tests were run in the flow facility discussed in reference 16.



(a) Wire form transpiration cooling material.



(b) Full coverage film cooling material.

Figure 14. - Surfaces of transpiration and film cooling materials.

Figure 14(a) shows a photograph of a piece of wire wound transpiration cooling material.

Fluid flow through the porous walls of a transpiration cooled structure can be described by the so-called "Green equation" given by

$$\frac{(p_1^2 - p_2^2)g}{\tau\mu^2(2RT)} = \alpha\left(\frac{G}{\mu}\right) + \beta\left(\frac{G}{\mu}\right)^2 \quad (1)$$

where α is a viscous resistance coefficient defining the viscous shear losses and β is an inertial resistance coefficient defining the losses cause by the tortuous cooling passages. (All symbols are defined in the appendix.)

Equation (1) can be rewritten in the form

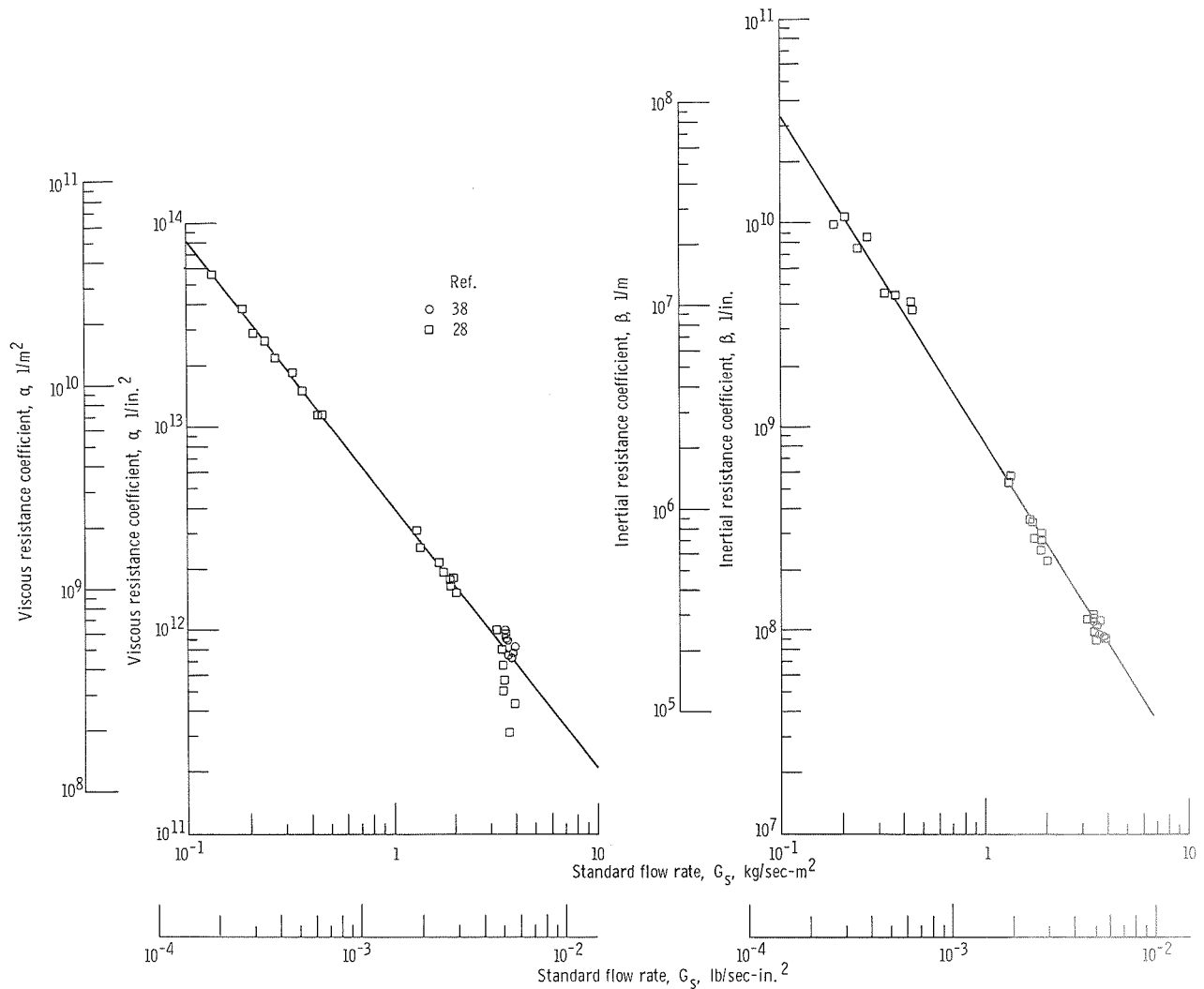
$$\frac{(p_1^2 - p_2^2)g}{\tau\mu(2RTG)} = \alpha + \beta\left(\frac{G}{\mu}\right) \quad (2)$$

The α and β coefficients can be determined, for a particular porous structure, by measuring flow rates through the wall under several different combinations of upstream and downstream pressures and plotting the data in terms of the parameter on the left of equation (2) against G/μ . According to equation (2), the data should fall on a line of intercept α and slope β . Thus, the flow through a porous wall is characterized by α and β .

In order to use equation (2) for analytical design purposes, where the required porous configuration is initially unknown, it is necessary to find some unique relationship between the resistance coefficients and some other parameter which can be used to specify the porous configuration. One such parameter is G_S , the mass flow rate per unit area under a set of standard conditions, defined in the symbols list. Most wire-form porous sheets for vane or blade transpiration cooling is ordered from the manufacturer by the G_S value.

The viscous and inertial resistance coefficients from Allison and NASA flow test of wound wire-form porous sheet (see refs. 28 and 38) are presented in figure 15 as logarithmic functions of G_S . From the straight line plots of data in figure 15, the following exponential equations for α and β as functions of G_S were obtained:

$$\alpha = 39.7(10^8)(G_S 10^3)^{-1.29} \quad (3)$$



(a) Viscous resistance coefficient correlation.

(b) Inertial resistance coefficient correlation.

Figure 15. - Wire-form porous sheet flow data correlation as function of G_S .

and

$$\beta = 35.6(10^5)(G_S 10^3)^{-1.61} \quad (4)$$

Equations (3) and (4) are in U.S. Customary units. In SI units, they become

$$\alpha = 61.5(10^{11})(703G_S 10^3)^{-1.29} \quad (5)$$

and

$$\beta = 140.3(10^6)(703G_S 10^3)^{-1.61} \quad (6)$$

These results were derived from room-temperature flow tests on flat specimens. Further work proved that flows could be predicted from equation (1), combined with equations (3) and (4) using fluid temperatures up to 700 K (800^o F) and sheet radii of curvature as low as 0.025 centimeter (0.10 in.).

Equation (2) may be rewritten as

$$C_f = \frac{(p_1^2 - p_2^2)g}{\beta RT \tau G^2} = \frac{2}{Re} + 2 \quad (7)$$

where

$$Re = \frac{G}{\mu} \frac{\beta}{\alpha} \quad (8)$$

and β/α has the dimension of length.

Flow data plotted according to equation (7) will fall on a single curve. Such a plot was not made herein, however, for wound wire-form porous sheets.

Full Coverage Film Cooling

Laminated sheet metal. - As for the transpiration cooled vane, a knowledge of flow characteristics is necessary in order to design a full-coverage film cooled vane. Flow studies were made by the Detroit Diesel-Allison Division of General Motors Corporation (contract NAS 3-12431) and are reported in references 28 and 29. The flow tests were performed in the same way as those for transpiration cooling.

Fifteen different internal flow configurations were considered by testing disks as shown in figure 14(b) in a flow facility. The disks for a given internal configuration were cut from different sheets of the material in order to determine uniformity of fabrication. Flow data presented in reference 28 with $(p_1^2 - p_2^2)g/\tau\mu 2RT$ plotted against G/μ yielded separate curves for each specimen tested. Details of the differences in geometry of the 15 samples tested and the ranges of variables considered in the investigation are given in reference 28. Tests were run with both ambient and 422 K (300^o F) temperature air and

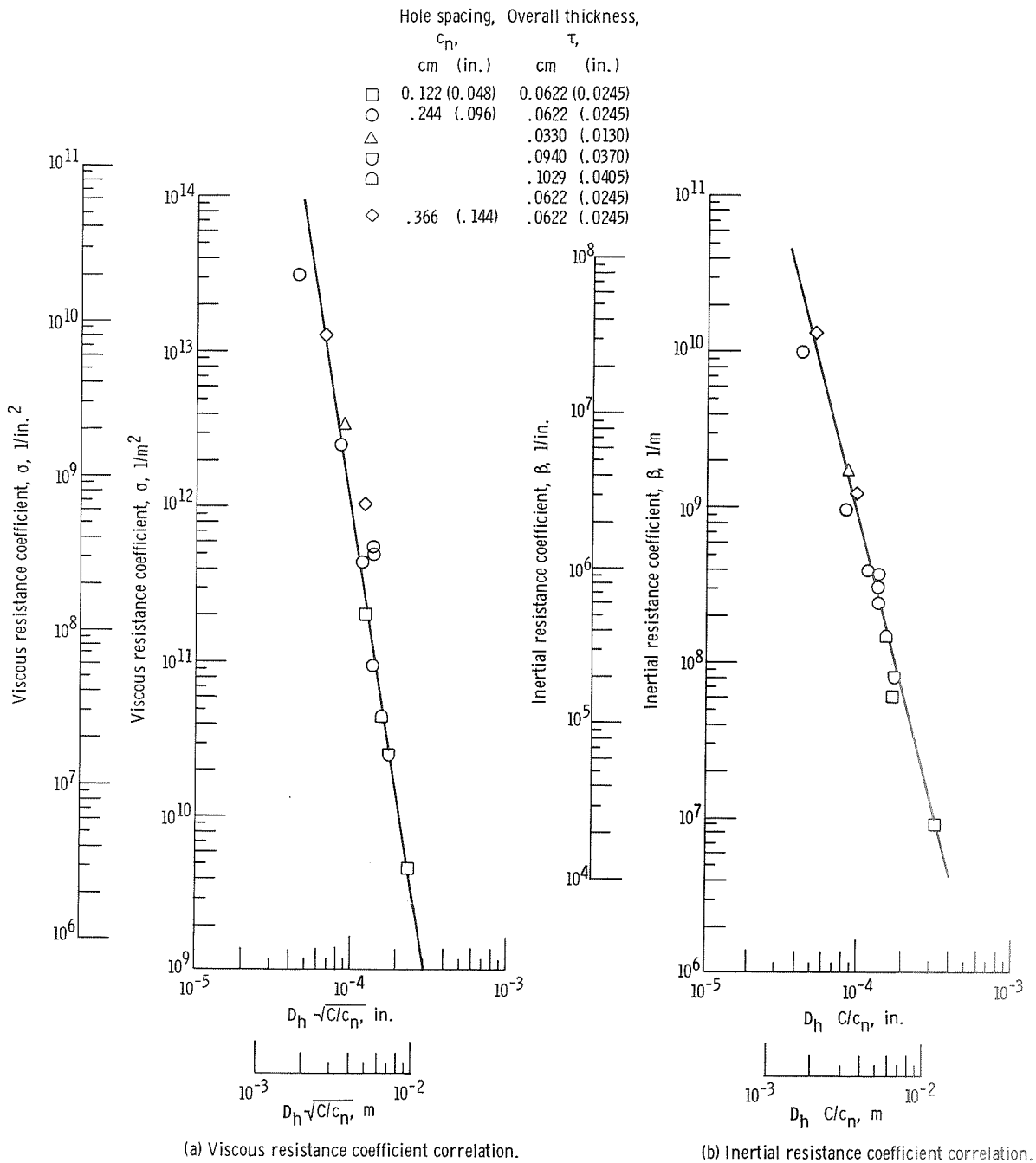


Figure 16. - Laminate-form porous sheet flow data correlation as function of hydraulic diameter D_h and hole spacing c_n .

no differences in flow characteristics were observed. Although the data were also plotted according to equation (7), this correlation is of no use for design purposes unless α and β are known, and α and β had to be obtained from the individual plots for each specimen (as intercept and slope respectively).

The data from the individual specimen plots were successfully correlated at Lewis in a manner similar to that just discussed for wound wire-form porous material. These results are reported in reference 38. For this correlation, it was found that use of the hydraulic diameter D_h of the minimum flow area and of the spacing between holes c_n in square array would result once again in linear plots on log log scale. The viscous resistance coefficient α was plotted against $D_h \sqrt{C/c_n}$ and the inertial resistance coefficient β was plotted against $D_h C/c_n$ where C is a constant (0.0024 in SI units and 0.096 in U.S. Customary units). The plots are shown in figure 16.

From the figure, the following correlation equations were obtained:

$$\alpha = 1.7(10^6) \left[D_h \sqrt{\frac{0.096}{c_n}} (10^2) \right]^{-6.34} \quad (9)$$

and

$$\beta = 0.6(10^5) \left[D_h \left(\frac{0.096}{c_n} \right) (10^2) \right]^{-3.9} \quad (10)$$

in U.S. Customary units and

$$\alpha = 2.6(10^9) \left[D_h \sqrt{\frac{0.00244}{c_n}} (10^2) \right]^{-6.34} \quad (11)$$

and

$$\beta = 23.6(10^5) \left[D_h \left(\frac{0.00244}{c_n} \right) (10^2) \right]^{-3.9} \quad (12)$$

in SI units.

Figure 17, taken from reference 28, also shows the data correlated according to equation (7). However, as stated previously, this correlation is of no use in design work if values of α and β are not known. These values, however, can be calculated from equations (9) and (10) or equations (11) and (12).

A number of full-coverage film cooled vanes were made by the contractor. Before forming the vanes, the sheets of material were carefully flow checked, as reported in

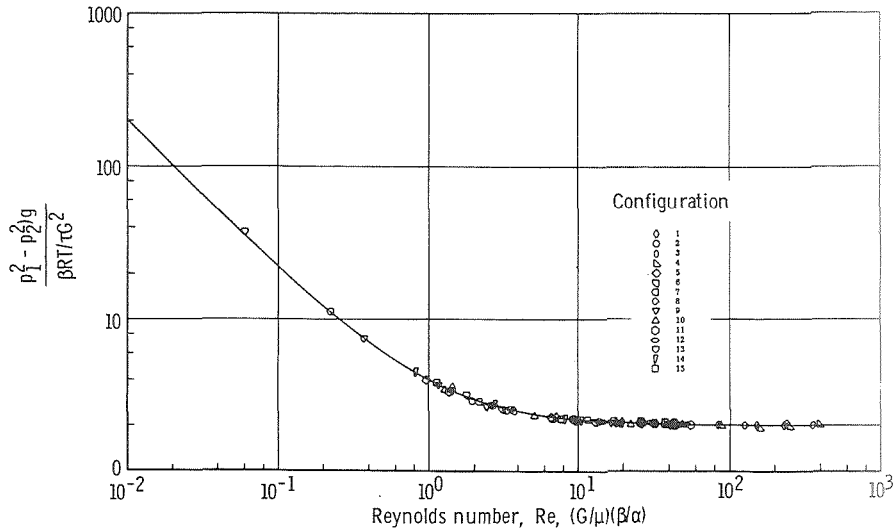
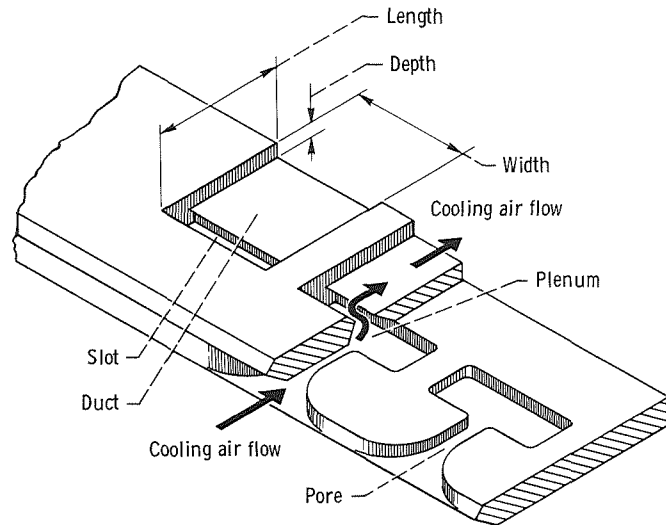


Figure 17. - Permeability data for full-coverage film-cooled laminated sheet material made by Detroit Diesel-Allison Division of General Motors Corporation (see table I; ref. 28).

reference 29. After fabrication of the vanes, two were selected as test vanes and detailed flow studies of these vanes were made at the midspan section and at sections 2.54 centimeters (1 in.) above and below the midspan section. Measurements were made at approximately 105 locations per vane. A soft plastic tube was attached to a transducer and was used for these measurements; the free end of the tube was placed against the vane surface and positioned so that no holes were blocked. The tube diameter was selected so that four holes on the suction surface or four holes on the pressure surface could be covered. A single hole was covered by a smaller tube at the leading edge.

Following heat-transfer tests in the high temperature cascade, the two vanes were again flow checked. Comparison of the pre- and post-cascade operation flow tests indicated the viscous flow coefficient α increased substantially during the cascade test. The inertial resistance coefficient β indicated a tendency to increase in the suction and leading edge regions and to decrease in the pressure surface region. For the ranges of conditions considered, the factor β has the greater influence on flow through the material and the factor α has only a secondary effect on the flow. In general, the average value of β increased during the testing period and thus reduced the flow through the vanes for a given pressure drop across the airfoil. For details of these flow tests and results, see reference 29.

Laminated platelets. - The full-coverage film cooled vanes were made from thin platelets with photoetched cooling air passages; these platelets were diffusion bonded together (see fig. 9(d)). Since no data were available for flow of air passing through photoetched passages, it was necessary to fabricate flow specimens of varying passage geometries to obtain sufficient flow data for vane design purposes. These specimens were



CD-11064-33
 Figure 18. - Full-coverage film-cooled laminated platelet configuration.

then tested in a flow test apparatus by Aerojet Liquid Rocket Company (contract NAS 3-10495). Reference 30 presents all details of this investigation.

Two types of flow specimens were designed: The first type was made of straight through passages, and the second type is shown in figure 18. From data obtained on flow tests of plastic models, the straight through samples showed that the cooling air did not spread across the slot; hence, the necessity for the second type became evident. It should also be pointed out that, because of difficulty in exactly duplicating similar etch dimensions, the data for the straight through specimens could not be correlated.

Only two specimens containing the pore-duct combination were considered; these two are of primary interest here. The parameters of these two flow specimens are:

Average depth of etch		Mean area per passage		Mean hydraulic diameter, D_h		Number of passages	Total specimen actual flow area	
cm	in.	cm ²	in. ²	cm	in.		cm ²	in. ²
4.826×10^{-3}	0.0019	6.877×10^{-5}	10.66×10^{-6}	6.782×10^{-3}	0.00267	931	6.406×10^{-2}	9.93×10^{-3}
5.334	.0021	11.581	17.95	7.518	.00296	931	10.774	16.70

Test were run for the following conditions:

Pressure ratio	Average inlet pressure		Discharge pressure		Average inlet pressure		Discharge pressure	
	N/m ²	psia	N/m ²	psia	N/m ²	psia	N/m ²	psia
1.07	1.083×10 ⁵	15.7	1.013×10 ⁵	14.7	3.17×10 ⁵	46.0	2.965×10 ⁵	43.0
1.2	1.218	17.65			3.56	51.6		
1.5	1.552	22.05			4.45	64.5		
2.0	2.030	29.40			5.94	86.0		

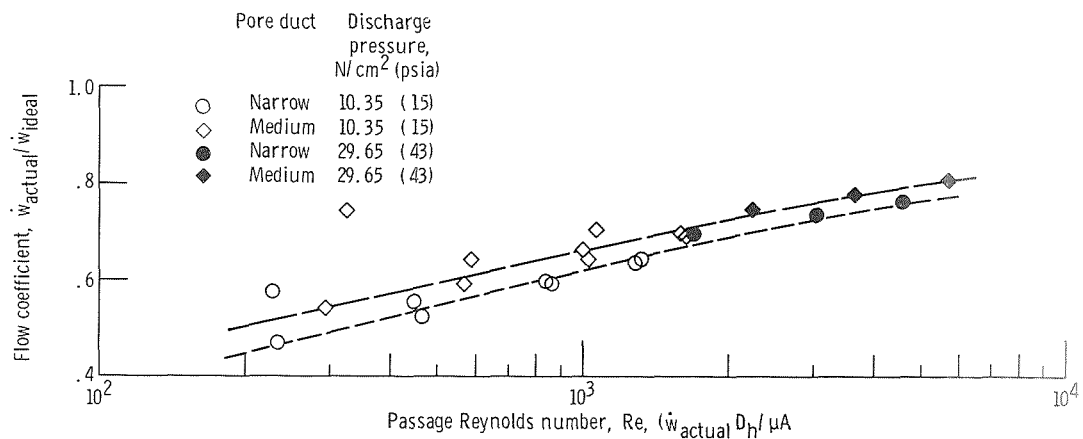


Figure 19. - Flow test results for photoetched full coverage film-cooled laminated platelet specimens.

The test results are shown in figure 19, plotted with the flow coefficient for the passage as a function of the passage Reynolds number. The flow coefficient (or ordinate) in figure 19 contains the pressure drop through the combination of pore, plenum, slot, and duct; the Reynolds number (or abscissa) is calculated with the pore hydraulic diameter as the characteristic dimension. It is not known at present whether the plenum and slot pressure drops are appreciable. If they are, the curves of figure 19 probably only apply to an overall geometry for which the curves were obtained. If these pressure drops are not appreciable, it still is undetermined whether D_h is the correlating parameter until a much wider range of D_h values than those given in figure 19 are tested. Consequently, more flow testing of such configurations is required.

HEAT-TRANSFER RESEARCH

The ultimate objective of the heat transfer investigations described herein is to develop correlations that can be applied generally to the design of cooled vanes and blades. When properly developed, such correlations could result in better designs that would not require so much developmental testing to qualify as flight hardware. To accomplish this objective, the analytically predicted cooling performance of vanes and blades designed from currently available correlations is compared with experimental performance determined under actual or simulated engine environments. Modifications or refinements are made in the current correlations to obtain good agreement between analytical and experimental results.

Heat-Transfer Experimental Data Correlation

A cooling correlation method has been devised whereby, for some cooling configurations the metal temperature data should approximate a simple curve regardless of gas temperature, cooling air temperature, and gas and coolant flow rates. The curve is obtained by plotting

$$\bar{\varphi} \text{ vs } \frac{\dot{w}_c}{\dot{w}_g} \quad (13)$$

where

$$\bar{\varphi} = \frac{T_{Ti} - \bar{T}_w}{T_{Ti} - T_{c,i}} \quad (14)$$

At this point it must be pointed out that investigations reported herein have been limited to the midspan section of the vane. The term \bar{T}_{ge} is usually used instead of T_{Ti} in the definition of $\bar{\varphi}$, where \bar{T}_{ge} is the integrated average of the chordwise distribution of local values of T_{ge} at the midspan section. However, the value of \bar{T}_{ge} is nearly equal to the value of the turbine inlet temperature at the leading edge of the midspan vane section; the difference between \bar{T}_{ge} and this inlet temperature is about 25° R. For ease in calculation and for use in design, the turbine inlet temperatures at the leading edge of the vane midspan section (T_{Ti}) is therefore used throughout this report as an approximation for \bar{T}_{ge} . The error in $\bar{\varphi}$ caused by the use of the turbine inlet temperature T_{Ti} at the vane midspan leading edge region for \bar{T}_{ge} is negligible. Throughout this report, the

measured wall temperatures were corrected for radiation effects to the water cooled wall by the method of reference 39. The correlation should be valid for a complete vane, or for a section of a vane such as the leading edge region.

Data obtained for the midspan section of the vane shown in figure 4 and operated in the static cascade shown in figure 6 are plotted in figure 20 for a range of operating conditions. The solid curve represents a best fit through all the data. The data for the high coolant inlet temperatures are on the order of 10 percent higher than those for the low coolant inlet temperatures.

Plots like that of figure 20 are very useful. The plots can be obtained with a minimum amount of testing over a limited range of variables and can be used to estimate metal temperatures over any range of variables. The method can be applied to either vanes or blades and can be used to compare the cooling effectiveness of different vanes or of different blades. The method is entirely independent of the method of scaling low temperature data to high temperature cases, to be discussed next.

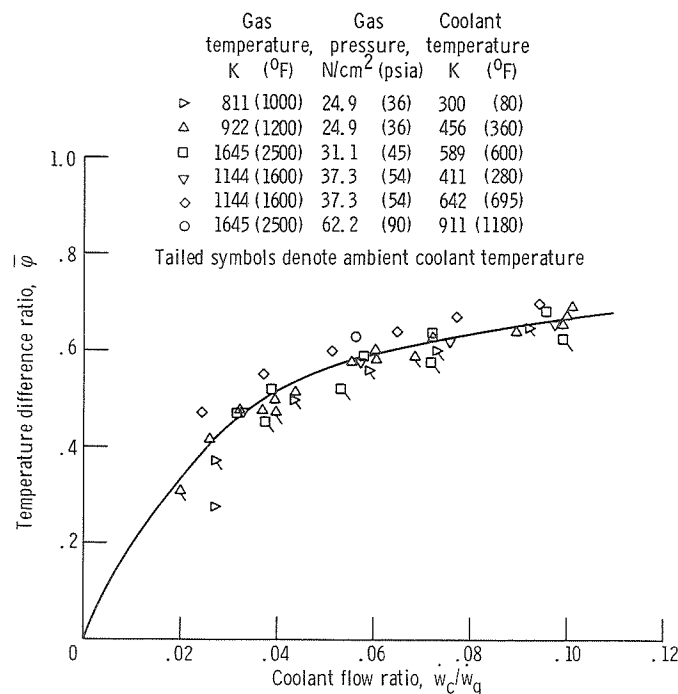


Figure 20. - Heat-transfer data for film-impingement-cooled vane operated in static cascade.

Scaling Low-Temperature Results to High-Temperature Conditions

Vanes and blades of various cooling configurations have been tested in the static cascade and the research engine described previously. Some examples of the experimental vane temperature data obtained from these tests are given below.

Experimental heat-transfer investigations of cooled vanes and blades at high gas stream temperatures are costly and time-consuming because of the deteriorating effects of the test environment on the test apparatus and the associated instrumentation. For example, thermocouples that can be used on thin-walled vanes and blades are necessarily small (approx. 0.0076 cm (3 mils) diam.). These small diameter wires are highly susceptible to failure when subjected to the effects of hot gas streams. To conserve the service life of test apparatus and instrumentation, use of the similarity parameter $\bar{\varphi}$ is made; $\bar{\varphi}$ obtained from experimental vane temperature data obtained at low gas and coolant temperature levels is used to predict vane temperatures that would occur at higher levels of gas and coolant temperatures.

A comparison of scaled and experimental data for the vane shown in figure 4 is presented in figure 21. The experimental data (circles) shown on the lower part of this figure were obtained during cascade operations. The operating conditions were a gas tem-

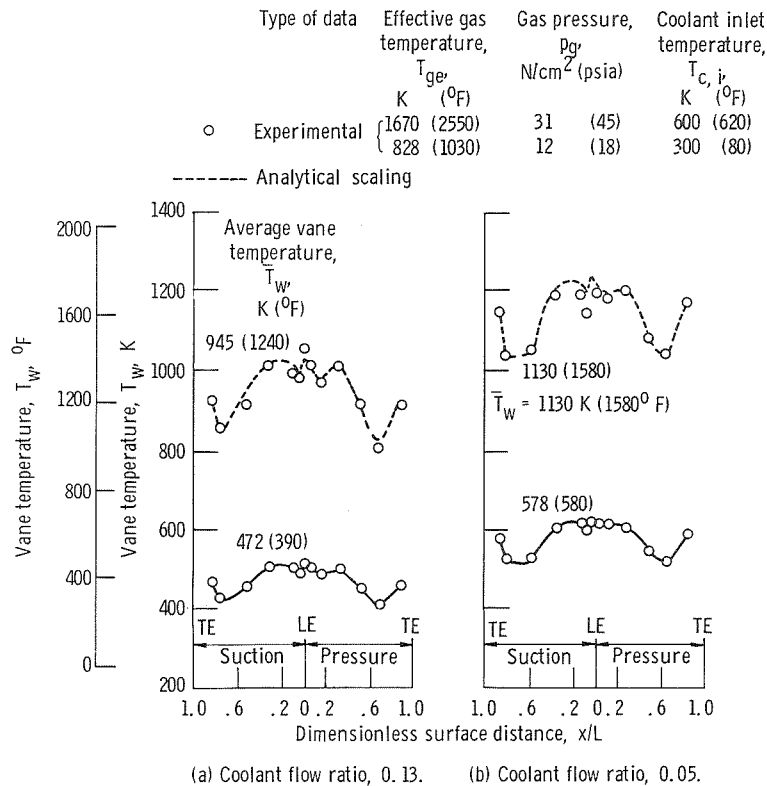


Figure 21. - Comparison of high temperature data with scaled results obtained from low temperature data.

perature of 828 K (1030^o F), a gas pressure of 12 newtons per square centimeter (18 psia), and a cooling air temperature of 300 K (80^o F). The solid lines were drawn through these experimental data, the lower left for a coolant to gas flow ratio of 0.13, and the lower right for the ratio 0.05. The average vane temperature under these environmental conditions was 472 K (390^o F) for the higher flow ratio (left) and 578 K (580^o F) for the lower flow ratio (right). To predict the vane temperatures at higher gas and cooling air temperature levels, it was assumed that the gas Reynolds number, the gas pressure coefficient, the coolant Reynolds number, and the coolant flow ratio \dot{w}_c/\dot{w}_g were constant for both cases. A gas temperature of 1670 K (2550^o F) was selected for the high-temperature case. From the ratio of coolant to gas viscosities at the low temperature level, the corresponding value of the coolant temperature was determined to be 600 K (620^o F). Then, by assuming a constant ratio of the difference between the gas turbine inlet and inlet coolant temperatures, that is, $\bar{\varphi} = \text{constant}$, the scaled value of the average vane temperature was determined to be 945 K (1240^o F) for the high flow ratio (left), and 1130 K (1580^o F) for the low flow ratio (right). Also, by using the local temperature difference ratios φ the local vane temperatures were determined. These scaled distributions of local vane temperatures are shown by the dashed lines at the top of figure 21. The validity of the data scaling was checked by experimentally testing the vane at the conditions that were assumed for the scaling. The experimental local vane temperatures are shown by the symbols in the upper part of figure 21. The agreement between experimental and scaled temperatures is very good. This agreement shows that this scaling method can be used for preliminary experimental evaluation of the cooling performance of vanes and blades designed for high temperature application without using the high temperature environment.

Cooling Comparison of Vanes

Experimental heat-transfer results were obtained for some of the vanes discussed previously. Data were obtained from tests of (1) the film-convection cooled vane of figure 9(a) in the turbine cooling research engine of figure 8, (2) the film-impingement cooled vane of figure 9(b) in the static cascade of figure 6, and (3) the full-coverage film cooled vane of figure 9(c) from tests in another high temperature cascade. The full-coverage film cooled tests were run by the Detroit Diesel-Allison Division of the General Motors Corporation in their cascade and are reported in reference 29.

Figure 20 shows the data obtained for the film impingement cooled vane and figure 22 the data for the film-convection cooled vane. The data are plotted with $\bar{\varphi}$ as ordinate and \dot{w}_c/\dot{w}_g as abscissa. The value of $\bar{\varphi}$ is a measure of the heat exchanger effectiveness of the cooling configuration. Data for ranges of operating conditions are shown in each figure, and best fit curves are drawn through the data. These best fit curves are

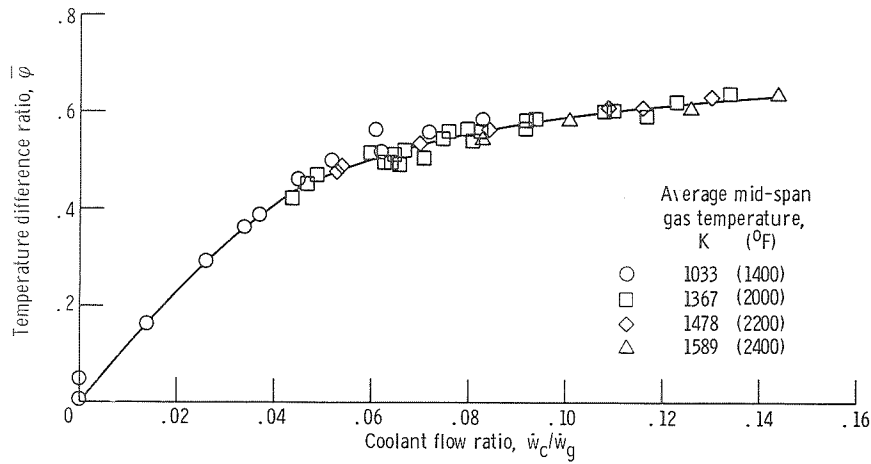


Figure 22. - Heat-transfer data for film-convection cooled vane operated in research engine.

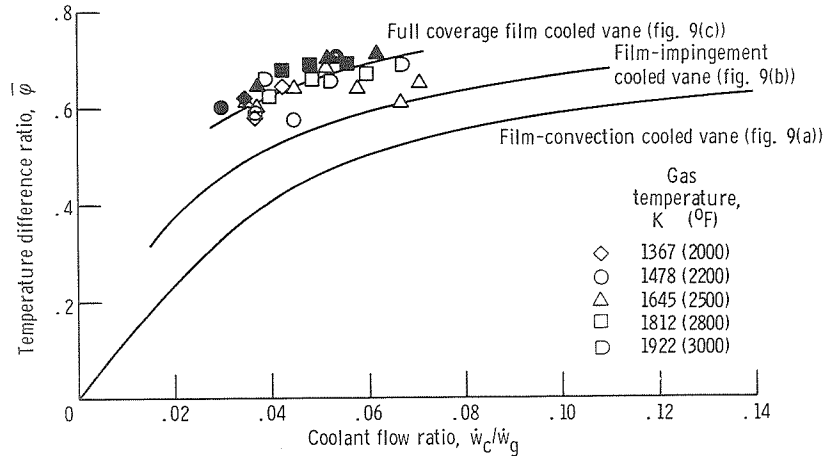


Figure 23. - Comparison of film-convection, film-impingement and full-coverage film-cooled vanes.

reproduced in figure 23 which also contains the data obtained by the Detroit Diesel-Allison Division of General Motors Corporation for the full-coverage film cooled vane tested in the Allison high temperature cascade and a best fit curve through these data. From figure 23 it can be seen that the full-coverage film cooled vane is superior to the film-impingement and the film-convection cooled vanes. For example, for a coolant flow ratio $\dot{w}_c/\dot{w}_g = 0.05$, a value of $T_{Ti} = 1645 \text{ K} (2500^\circ \text{ F})$ and $T_{ci} = 811 \text{ K} (1000^\circ \text{ F})$ the values of \bar{T}_{w} , obtained by calculation from the data in figure 23 are $1261 \text{ K} (1810^\circ \text{ F})$, $1179 \text{ K} (1660^\circ \text{ F})$, and $1095 \text{ K} (1510^\circ \text{ F})$ for the film-convection, film-impingement, and full-coverage film cooled vanes, respectively.

Figure 24 is a plot of vane midspan allowable turbine inlet temperature against coolant flow ratio. It was constructed for a maximum wall temperature $T_{w,max}$ of 1367 K

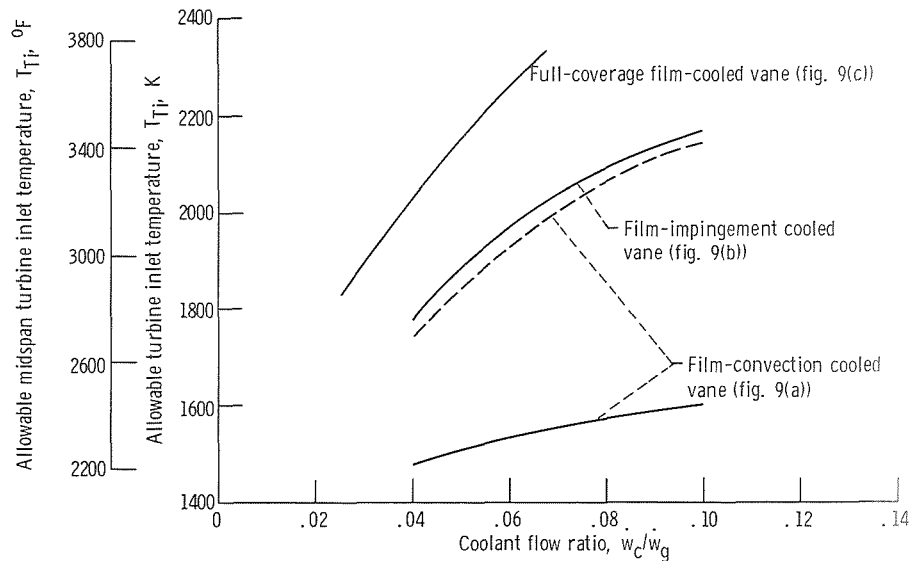


Figure 24. - Allowable midspan turbine inlet temperature as function of coolant flow ratio for full-coverage film, film-impingement, and film-convection cooled vanes. Maximum wall temperatures, 1367 K (2000° F); coolant inlet, 811 K (1000° F).

(2000° F) and a coolant inlet temperature of 811 K (1000° F) by cross plotting data from a figure like figure 23 with the maximum hot spot wall temperature used instead of the average wall temperature in the ordinate. For a coolant flow ratio of 0.05, the figure shows that the value of T_{Ti} can be increased from 1510 K (2258° F) for the film-convection vane to 1880 K (2924° F) for the film-impingement vane and to 2150 K (3410° F) for the full-coverage film cooled vane.

Figure 24 shows that the full-coverage film cooled vane is more effective from a heat transfer standpoint than the other two vanes. However, this superiority of the full-coverage film cooled vane must be viewed with caution. Preliminary tests on the effect of cooled air leaving the vane and entering the hot gas stream have shown a decrease in the aerodynamic performance of the vane, particularly near the vane leading and trailing edge regions on the suction surface (see ref. 40). More work on the effect of this cooling air bleed into the gas stream on aerodynamic performance is required, particularly in the vane regions noted previously, in order to eliminate or at least minimize this detrimental effect. In addition, another factor of importance relative to full-coverage film cooling is the effect of oxidation on this type of cooling. Oxidation effects will be discussed in a latter section of this paper.

Some remarks about the film-convection vane curves in figures 23 and 24 are in order. The test data showed excessive chordwise temperature gradients in this vane. In other words, the cooling air was not distributed in the optimum proportion between the leading edge and midchord coolant passages. The leading edge of the vane was not cooled sufficiently, and the midchord region was overcooled. A more effective redistribution of

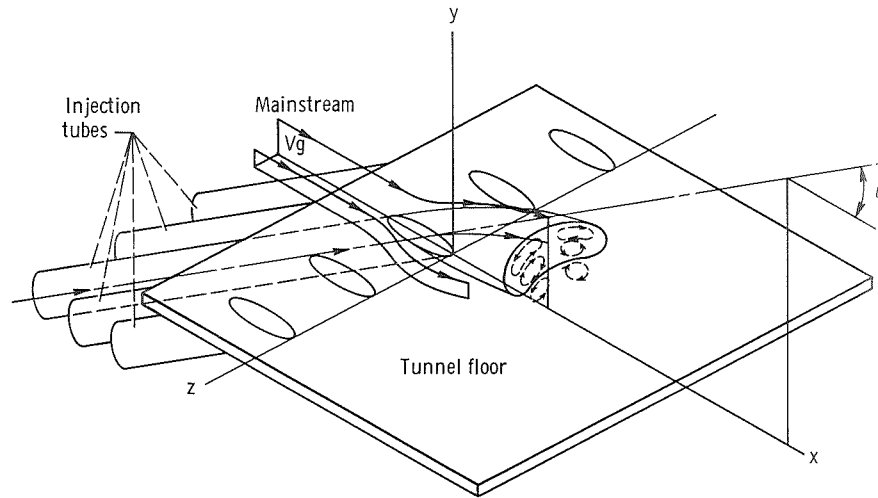
the cooling air would lower the leading edge region temperatures and raise the midchord region temperatures. The film-convection curve in figure 24 was constructed for the highest temperature of the vane. If a redistribution of cooling air can be achieved so that the chordwise vane temperature gradient can be eliminated (i. e. , a uniform vane temperature) while assuming the same cooling effectiveness, the film-convection curve in figure 24 would be replaced by a new curve - the dashed curve in figure 24. This dashed curve is for an ideal case, and the entire potential gain probably never can be obtained. Such a comparison does illustrate that, with proper redistribution of the cooling air, the film-convection cooled vane can be greatly improved.

Although figure 24 shows that the film-impingement vane is somewhat more effective than the film-convection cooled vane, problems in fabrication of the vanes must be considered. It may turn out that one type is more feasible to fabricate than the other, particularly when the vane size decreases, an almost certain trend for future engines. Which of these two types of vanes to be used in a certain engine application must be decided by the engine manufacturer.

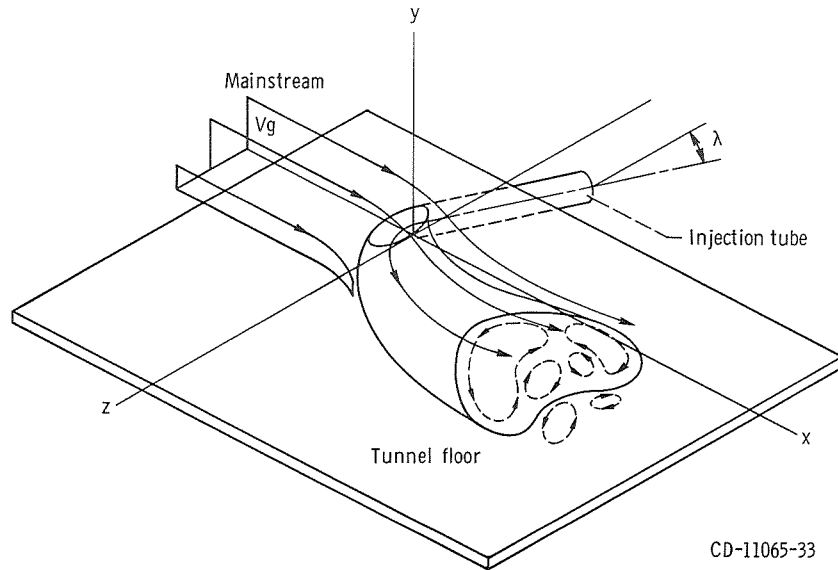
Thus far, the heat-transfer results have all dealt with experimental data and the correlation of these data. Ideally, however, the ability to predict heat-transfer coefficients and, in turn, accurate metal temperatures for the different cooling schemes is desired. The next several sections of this paper are aimed at supplying typical information useful in the prediction of accurate metal temperatures.

Film Cooling

Fundamental film cooling studies on a flat plate in a tunnel with a secondary gas flowing through a single hole and through rows of discrete holes are being carried out at the University of Minnesota under contract NAS 3-13200. References 3, 6, and 41 present some of the results of film cooling studies made under contract NAS 3-7904; reference 3 refers to single holes, reference 6 to both single holes and rows of discrete holes, and reference 41 includes surveys of velocity and temperature profiles and measurements of turbulence intensity. Figure 25(a) shows the injection segment and coordinate system for a row of inclined jets, with the detail of the flow field shown for only a single jet interaction with the mainstream, and figure 25(b) shows the flow field and coordinate system associated with a laterally inclined jet interacting with a mainstream. The injection angle of the flow ψ is measured from the x axis in the x - y plane. Values of ψ of 35° and 90° were considered. For the row of holes, ψ was fixed at 35° , and the discrete holes were spaced at intervals of 3 hole diameters. Single tubes were also studied for lateral injection angles λ of 35° and 15° ; λ is measured from the z axis in the yz plane (see fig. 25(b)).



(a) Injection segment and coordinate system for row of inclined jets. Detail and flow field are shown for only a single jet interacting with a mainstream.



(b) Flow field and coordinate system associated with a laterally inclined jet interacting with a mainstream.

Figure 25. - Flow field and coordinate system for film cooling.

A description of the flow field shown in figure 25 was presented in reference 41 and is reproduced herein. As the jet enters, it leaves a void (low pressure condition) downstream of it which is filled by mainstream air moving around the jet. In the region near the wall and for a distance almost halfway around the jet the flow patterns look similar to what is found around a cylinder in cross flow. The flow continues around the jet and into the apparent low pressure region on its downstream side.

At high blowing rates ($M = \rho_c v_c / \rho_g v_g > 1$) the mainstream air moves into the region immediately downstream of the injection location parallel to the floor of the tunnel and laterally with almost no component of velocity in the downstream direction. As the mainstream air moves towards the zero lateral position ($z/D = 0$) it begins to move upward away from the wall, apparently being entrained by the jet. This region where the air enters from the side and then moves vertically extends approximately two diameters downstream and is a region of extreme fluctuations.

Approximately one diameter downstream, as the air moves vertically away from the wall, it reaches a height where it turns upstream and reverse flow exists. At greater distances from the wall the flow changes from reverse to forward flow. The inclination of the jet relative to the mainstream direction reaches zero between 2.5 and 3 diameters from the wall.

Farther downstream the flow, after rising from the wall, turns downstream rather than upstream and lateral components are also observed, indicating the possible formation of vortices. The outer portion of the vortex flow becomes overwhelmed by the main flow and the lateral velocities appear to diminish rapidly. At distances greater than two diameters downstream, the lateral velocity components diminish with axial distance until at approximately ten diameters no lateral velocity is observable.

For lower blowing rates, the trends are the same as those for the higher injection rate, the mainstream flow being drawn in to fill the void on the downstream side of the jet, this flow moving inward and then upward. Finally, depending on the axial position, the flow moves either upstream (reverse flow) or downstream and is then entrained by the jet. The principal difference between the flow patterns of the two extremes in blowing rates is that at the lower injection rate the vertical components of velocity in all regions are smaller.

In the heat-transfer tests adiabatic wall temperatures were investigated at both axial and lateral distances from the injection holes. The effect of the blowing parameter and the influence of the ratio of the turbulent boundary layer displacement thickness to hole diameter at the point of injection were considered. For these studies, the temperature of the injected air was 328 K (131° F) higher than the mainstream temperature. Free-stream velocities from 30.5 to 61 meters per second (100 to 200 ft/sec), displacement thickness of the turbulent boundary layer at the injection point from 0.121 to 0.135 centimeter (0.307 to 0.343 in.) and blowing parameters M from 0.1 to 2 were investigated.

From measured values of the adiabatic wall temperature and the known values of the gas and coolant inlet temperatures, values of the film cooling effectiveness η_{film} where

$$\eta_{\text{film}} = \frac{T_{\text{ge}} - T_{\text{aw}}}{T_{\text{ge}} - T_{\text{c},0}} \quad (15)$$

were evaluated. Figure 26 shows a typical plot of η_{film} against the dimensionless distance downstream from the injection hole for both a single hole and a single row of five holes. A range of dimensionless lateral distances from the injection hole was included. The figure is for an injection angle of 35° , a blowing parameter value of 0.5, injection holes of diameter D of 1.18 centimeter (0.464 in.), mainstream flow rate of 30.5 meters per second (100 ft/sec), and a gas Reynolds number $Re_g = v_g D / \nu_g$ of 0.22×10^5 . Reference 6 presents data for many other conditions; for example M from 0.1 to 2, $Re_g = 0.44 \times 10^5$, etc. The figure shows that the results for a single injection hole and for five injection holes are essentially the same until a lateral distance from the injection holes of 1.5 hole diameters is reached. When $z/D = 1.5$, the figure shows that the five hole arrangement is slightly superior to the single hole. The film cooling effectiveness decreases as the lateral distance from the injection holes increases and also as the distance downstream from the injection hole increases.

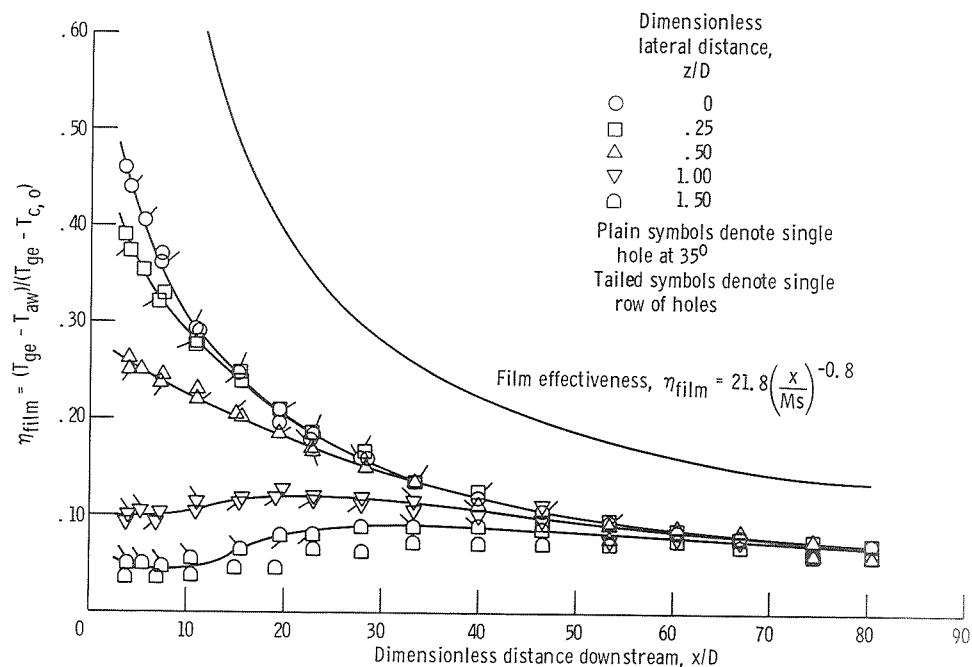


Figure 26. - Film-cooling effectiveness as function of dimensionless downstream and lateral distances from injection holes. Film blowing parameter, 0.5; injection hole diameter, 1.18 centimeter (0.039 ft); gas velocity, 3.05×10^5 centimeters per second (100 ft/sec); Reynolds number, $(v_g D_{\text{tube}} / \nu_g)$, 0.22×10^5 .

The upper curve in figure 26 is the effectiveness for a slot as first presented by Wieghardt (ref. 42) in the study of hot air discharge for deicing. This relation is

$$\eta_{\text{film}} = 21.8 \left(\frac{x}{Ms} \right)^{-0.8} \quad (16)$$

where s is the slot width. By equating the area of a row of injection holes to that of an equivalent slot, equation (16) can be rewritten as

$$\eta_{\text{film}} = 21.8 \left(\frac{M \frac{\pi D}{4 \text{ spacing}}}{\frac{x}{D}} \right)^{0.8} \quad (17)$$

For the present case the upper curve in figure 26 was generated for $M = 0.5$ with the spacing equal to $3D$. Figure 26 indicates that more effective film cooling can be

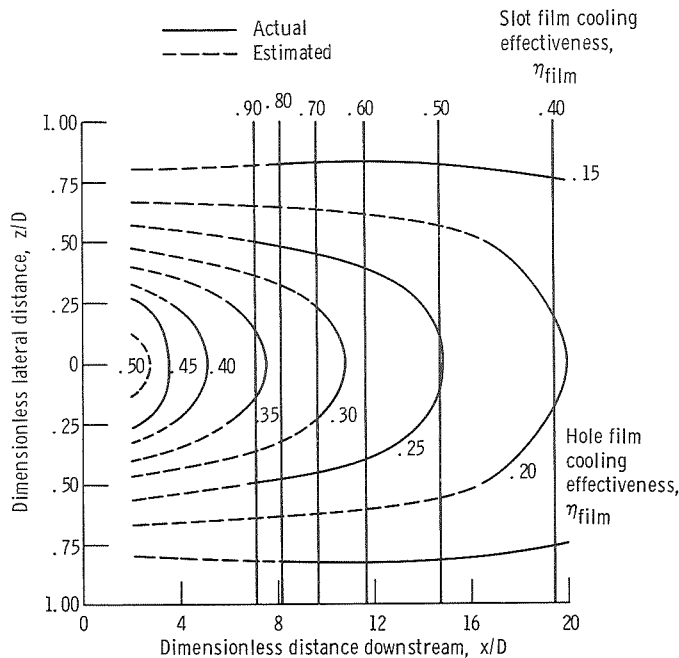


Figure 27. - Comparison of film cooling for discrete holes and for equivalent slot. Conditions for single tube at 35° : film blowing parameter, 0.05; tube diameter, 1.18 centimeters (0.039 ft); gas velocity, 3.05×10^3 centimeters per second (100 ft/sec); Reynolds number, 0.22×10^5 ; hole film-cooling effectiveness calculated from $(T_{g,e} - T_{aw}) / (T_{g,e} - T_{c,i})$. Conditions for one slot equivalent to a single row of five holes: Assumed 3 diameter spacing; slot film-cooling effectiveness calculated from $21.8 (x/Ms)^{-0.8}$.

achieved by use of a slot than by a row of discrete holes.

Figure 27 is a crossplot of figure 26 with the dimensionless lateral distance from the injection hole plotted against the dimensionless downstream distance from the injection hole and the film cooling effectiveness as a parameter. The solid parts of the curves are the values obtained from figure 26; the dashed continuations are estimated values. The solid vertical lines represent the results obtained by use of Wieghardt's equation for a slot (an equivalent slot was used, as discussed previously).

Figure 27 shows a decrease in film cooling effectiveness in both the lateral and downstream directions and the superiority of a slot as compared to a row of discrete holes. The figure shows that a slot is about twice as effective as discrete holes in the downstream direction from the holes.

Figure 28 shows contours of constant film cooling effectiveness for $M = 0.5$ through a single hole. The curves were determined by an interpolation scheme that fits quadratic equations to sets of three data points. Figure 28(a) is for an injection angle ψ of 35°

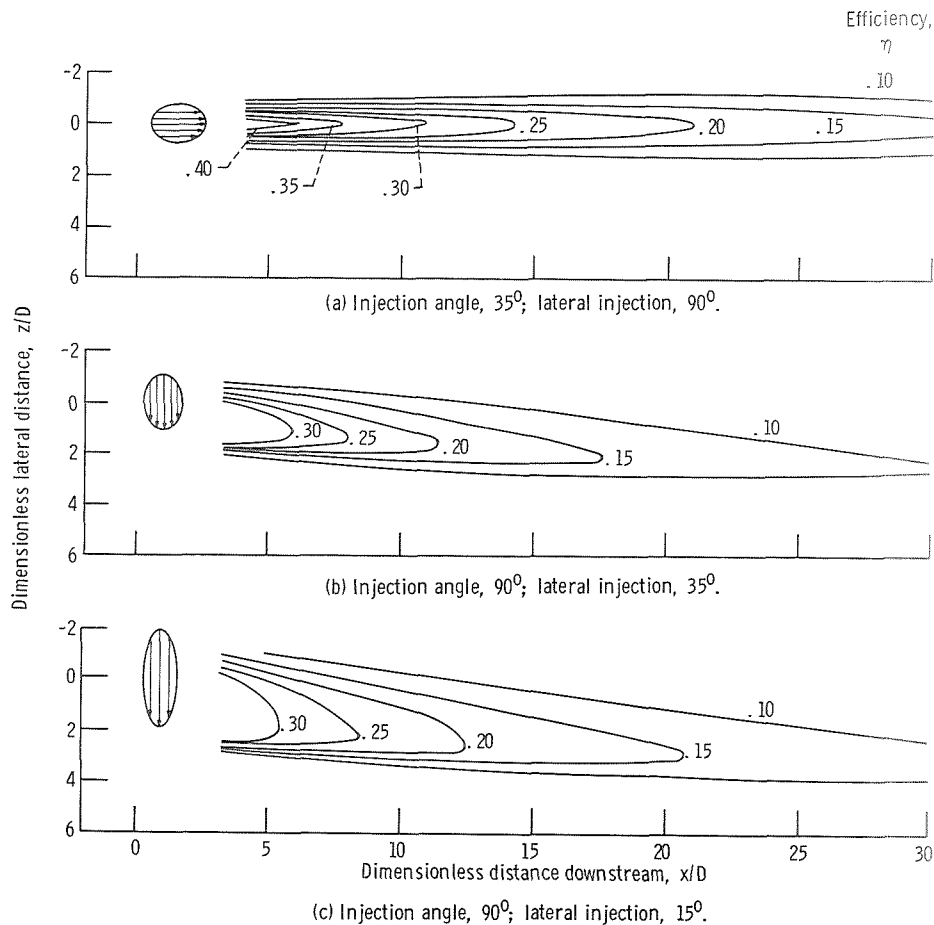


Figure 28. - Lines of constant film cooling effectiveness for single hole injection. Film blowing parameter, 0.5.

and lateral injection λ of 90° ; part (b) for $\psi = 90^\circ$ and $\lambda = 35^\circ$; and part (c) for $\psi = 90^\circ$, $\lambda = 15^\circ$. The figure (for $M = 0.5$) shows that lateral injection through a single hole widens the temperature field and decreases the peak effectiveness.

The experimental film cooling studies are required because of a lack of understanding of film cooling flow and heat-transfer characteristics. Hence, the empirical approach is necessary. To date, the effects of different variables on cooling effectiveness (or adiabatic wall temperature) and on the temperature and velocity fields of the jet and the mainstream have been investigated. The investigation is continuing in an effort to develop a semi-empirical analytical model useful for predicting jet temperature and velocity fields and cooling effectiveness. Methods for correlating data on cooling effectiveness for a large range of conditions and variables are also being investigated. Finally, the test apparatus will be modified in order to obtain data in which heat transfer exists across the film cooled wall and to determine if the relationship $q = h_{\text{conv}}(T_{\text{aw}} - T_w)$ holds for film cooling.

An independent investigation of film cooling was performed at Arizona State University. In reference 4, it is pointed out that in the region near injection, heat-transfer rates cannot be satisfactorily predicted with primary stream heat-transfer coefficients and adiabatic wall temperature distributions alone. As a consequence, the Arizona State University studies concentrated on obtaining experimental heat-transfer rates from a transient test facility. The tests were run for injection through flush angled slots into the turbulent boundary layer on a uniform temperature surface. The results are presented in reference 4 as the ratio of heat-transfer coefficient with film injection to that without film injection for three different injection angles by the following correlation ($1/4 \leq M \leq 1$ and $35 \leq l/s \leq 70$):

$$1.09 - 7.9\theta^* M^{0.6} \left(\frac{s}{l}\right)^{0.5} \quad \text{for } \psi = 20^\circ$$

$$\frac{h_{\text{film}}}{h_{\text{conv}}} = 1.18 - 7.5\theta^* M^{0.6} \left(\frac{s}{l}\right)^{0.5} \quad \text{for } \psi = 40^\circ \quad (18)$$

$$1.24 - 6.8\theta^* M^{0.6} \left(\frac{s}{l}\right)^{0.5} \quad \text{for } \psi = 60^\circ$$

where $\theta^* = (T_c - T_{ge}) / (T_w - T_{ge})$, s is slot width, and l is the length of the test surface from the slot exit in the downstream direction. Ranges of the variables applicable to turbine cooling were considered.

Reference 5 reports results obtained for slots and for holes and compares the results. The following 11 nozzle plates were tested:

Number of nozzles	Type of nozzles	Slot or hole width, S		Injection angle, ψ , deg	Spacing to diameter ratio, c_n/D
		cm	in.		
4	Slot	0.127	0.050	20	----
		.254	.100	60	----
4	Hole	0.127	0.050	20	1.71
		.254	.100	60	1.71
3	Hole	0.127	0.050	20	1.55
		.254	.100	60	1.55

When the results were plotted with $(T_c - T_{ge})/(T_{aw} - T_{ge})$ as ordinate and l/s as abscissa, the slots proved more efficient than the holes (a result previously noted in the University of Minnesota work). This is explained as follows: the space between the holes allows the mainstream to penetrate unmixed to locations on the surface and the individual jets penetrate upward into the mainstream, allowing the mainstream to mix in under the jet and thereby reducing its effectiveness.

Under a NASA contract, the General Electric Company explored various types of vane and blade cooling configurations that would be useful for advanced supersonic trans-

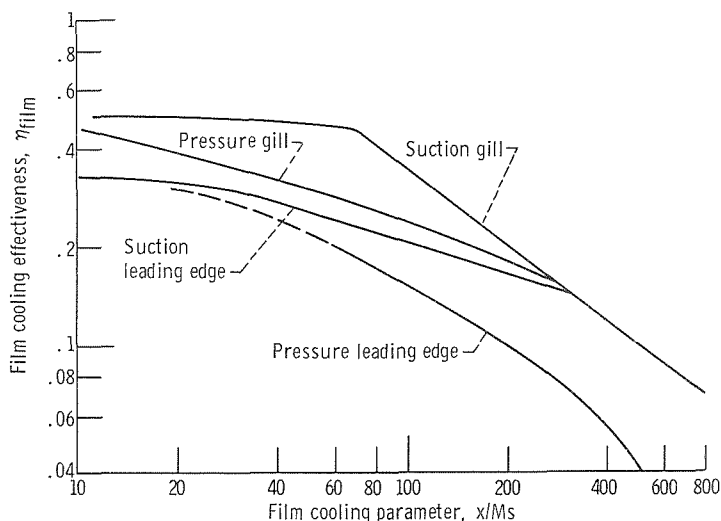


Figure 29. - Film-cooling effectiveness for vane analysis.

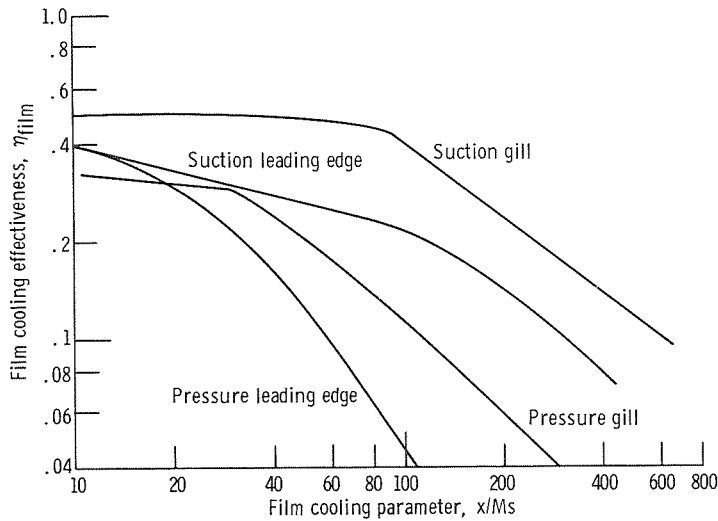


Figure 30. - Film-cooling effectiveness for blade analysis.

port applications. Convection, film, transpiration, and liquid metal cooling were all considered. The results of this study are given in reference 43 to 47. Attention here will be limited to the film cooling studies.

Figures 29 and 30 are plots of film cooling effectiveness obtained by the General Electric Company from tests on models similar to the vane and blade leading edges considered herein. According to reference 47, the gill region is that region close to the leading edge but removed from large variations in pressure. For values of $x/Ms \leq 100$, the data in figures 29 and 30 were able to be approximated by the following correlation equations:

Vane

$$\text{Leading edge - suction} \quad \eta_{\text{film}} = -0.002513 \left(\frac{x}{Ms} \right)^{0.878} + 0.35 \quad (19)$$

$$\text{- pressure} \quad \eta_{\text{film}} = -0.00667 \left(\frac{x}{Ms} \right)^{0.735} + 0.35 \quad (20)$$

$$\text{Gill - suction} \quad \eta_{\text{film}} = -0.00001 \left(\frac{x}{Ms} \right)^{1.952} + 0.5 \quad (21)$$

$$\text{- pressure} \quad \eta_{\text{film}} = -0.02626 \left(\frac{x}{Ms} \right)^{0.498} + 0.5 \quad (22)$$

Blade

$$\text{Leading edge - suction} \quad \eta_{\text{film}} = -0.0399 \left(\frac{x}{Ms} \right)^{0.38} + 0.45 \quad (23)$$

$$\text{- pressure} \quad \eta_{\text{film}} = -0.028 \left(\frac{x}{Ms} \right)^{0.577} + 0.45 \quad (24)$$

$$\text{Gill - suction} \quad \eta_{\text{film}} = -0.0000033 \left(\frac{x}{Ms} \right)^{2.13} + 0.5 \quad (25)$$

$$\text{- pressure} \quad \eta_{\text{film}} = -0.014 \left(\frac{x}{Ms} \right)^{0.654} + 0.5 \quad (26)$$

For values of $x/Ms > 100$, the curves of figures 29 and 30 were used in the calculations.

According to reference 1, many investigators assume that the film cooling heat-transfer coefficient is the same as with convection with T_{aw} used instead of T_{ge} and others assume a reduction in gas-to-surface heat-transfer coefficient due to film cooling. In reference 1, a modified transpiration cooling analysis was used to calculate the cooling air requirements for full coverage film cooling (the model had a large number of holes and hence the cooling approached transpiration cooling). It was assumed that h_{film} would be midway between h_{trans} and h_{conv} and that

$$\eta'_{\text{film}} = \frac{T_{c,o} - T_{c,i}}{T_{w,o} - T_{c,i}} = 0.6$$

In other words, it was assumed

$$\frac{h_{\text{film}}}{h_{\text{conv}}} = \frac{1}{2} \left(1 + \frac{h_{\text{trans}}}{h_{\text{conv}}} \right) \quad (27)$$

Values of $h_{\text{trans}}/h_{\text{conv}}$ were obtained from the transpiration cooling theory of reference 48:

$$\frac{h_{\text{trans}}}{h_{\text{conv}}} = \frac{B}{e^B - 1} \quad (28)$$

where

$$B = \frac{\overline{\rho_c v_c} c_{p,g}}{h_{conv}} \quad (29)$$

and where $\overline{\rho_c v_c}$ is the surface averaged mass velocity. This relationship was verified by experimental data on transpiration cooling in references 7 to 11.

In an attempt to verify that the assumption that h_{film} was midway between h_{trans} and h_{conv} , a check with some data reported in reference 6 was made. It was assumed that the heat transferred to the cooling air could be expressed as

$$\frac{\dot{w}_c c_{p,c}}{A} (T_{c,o} - T_{c,i}) = h_{conv} (T_{aw} - T_{w,o}) \quad (30)$$

By introducing the two values of η_{film} and η'_{film} as used in references 6 and 1, respectively, the preceding equation becomes

$$\frac{\dot{w}_c c_{p,c}}{A} = h_{conv} \left[\frac{1}{\eta'_{film}} \frac{T_g - T_{w,o}}{T_{w,o} - T_{c,i}} - \frac{\eta_{film}}{\eta'_{film}} \left(\frac{T_g - T_{c,i}}{T_{w,o} - T_{c,i}} - \eta'_{film} \right) \right] \quad (31)$$

and the flow parameter can then be obtained. By using $\eta'_{film} = 0.6$ and reading values of η_{film} from the top curve of figure 20 of reference 6 and estimating $\overline{\rho_c v_c}$ per hole as being $28 \overline{\rho_c v_c}$ (hole spacing of $5D$ inclined at a 35° angle) for the slanted holes, good agreement between the calculated values of the flow parameter and those in the abscissa of figure 20 of reference 6 was obtained.

Impingement cooling. - Fundamental studies of a linear array of circular jets impinging on the concave surface of a right semicylinder are being carried out at Newark College of Engineering under NASA contract NAS 3-1175. This contract is part of a NASA Lewis Research Center impingement cooling program, the ultimate goal of which is to develop design heat-transfer correlations to apply to cylindrically shaped leading edges of vanes or blades and for impingement cooling along the vane or blade suction and pressure surfaces. As mentioned previously, references 12 and 13 refer to related impingement cooling studies of the flow characteristics of a single jet impinging on a flat plate which were performed during the early stages of this impingement cooling program.

Reference 13 refers to a survey of literature on flow characteristics while reference 12 refers to experimental flow characteristics.

Since the Lewis contract with the Newark College of Engineering began, a number of investigations of jets impinging on the concave surface of a semicylinder have been reported in the literature (refs. 49 to 55). Some of these considered circular jets; others considered slots jets. Each reference presented a correlation equation for the data obtained during that specific investigation. These correlations are presented in table I. In an effort to determine how these correlations compared, the geometrical dimensions of the leading edge of the vane of figure 4 were considered. By using these dimensions, by adjusting the various correlations (basing each on an equivalent slot width) and by using a Reynolds number based on the nozzle exit velocity, an average Nusselt number applicable over a region of the vane leading edge extending $\pm 15^\circ$ on either side of the stagnation point was obtained; the results for five of the correlations are shown in figure 31.

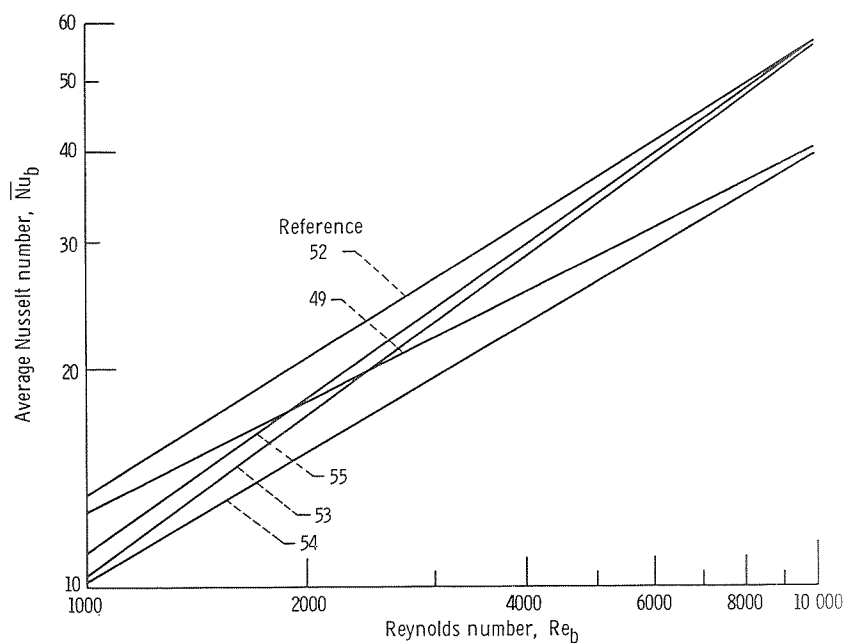


Figure 31. - Nusselt number as function of Reynolds number for linear array of equivalent slot jets as calculated from references 49 and 52 to 55.

At a relatively high leading edge Reynolds number, figure 31 indicates that the correlations can be separated into two groups. In the upper group are the correlations from references 52, 53, and 55 which were obtained from data for circular jets (the circular jets were replaced by an equivalent slot jet in fig. 31). In the lower group are the correlations obtained from references 49 and 54, based on data for slot jets. Figure 31 shows that, for relatively high leading edge Reynolds numbers, the three correlations for circular jets yield approximately the same \bar{Nu}_b and the two correlations for slot jets yield the

same but a smaller value of \bar{Nu}_b . Which correlation to use therefore depends on whether circular or slot jets are used in the particular application.

References 56 to 63 deal with impingement through arrays of circular jets on a flat plate. As before, each reference reports a specific correlation for the data obtained during the particular investigation. This type of impingement should be applicable to the suction and pressure surfaces of the midchord region of a vane. Using appropriate dimensions for the vane of figure 4, average Nusselt numbers were calculated for some of these correlations. Figure 32 presents the results of these correlations as applied to the

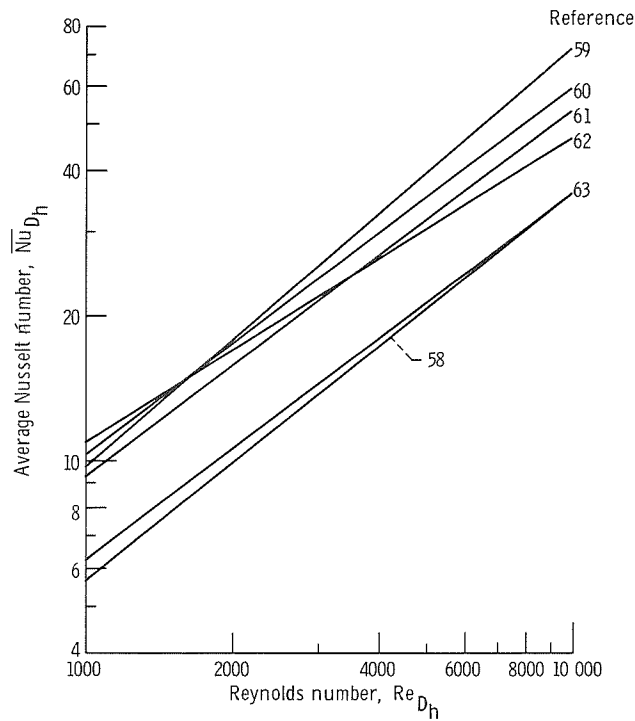


Figure 32. - Nusselt number as function of Reynolds number for two-dimensional array of circular jets as calculated from references 58 to 63.

vane of figure 4. It should be pointed out that impingement to the suction or pressure surface of a vane is affected by a crossflow set up by the air after it impinges on the surface and flows chordwise to a film cooling hole or a split trailing edge. The effects of a crossflow would tend to reduce the effectiveness of impingement cooling. Figure 32 does not account for any crossflow. However, the correlation presented in reference 58 has in it a term to account for crossflow effects; this term was evaluated for zero crossflow in the preparation of figure 32 so that a fair comparison of the correlations could be made. Suffice it to say that the line representing the correlation of reference 58 would

be lowered if crossflow effects were considered. More research on impingement cooling in the presence of a crossflow is required.

Effect of Chord Size on Coolant Requirements

Trend in blade size. - The trend in future engine designs is toward the core type of engine which has much higher gas temperatures and compressor pressure ratios than engines currently in use. The turbine vanes and blades of these core engines are much smaller than those used in present-day engines. These advanced engines will operate at temperatures up to 2480 K (4000⁰ F) and pressures as high as 414 newtons per square centimeter (600 psia) with blade spans of about 3.81 centimeters (1.5 in.). Future helicopter and lift engines will operate at less severe conditions with turbine inlet temperatures reaching 1645 K (2500⁰ F) at pressures of approximately 103 newtons per square centimeter (150 psia). However, these latter engines will have blades with spans of about 1.9 centimeters (0.75 in.).

Effect of chord size. - Because of these trends toward small-size turbine hardware, a study of the effect of blade size on the coolant requirement has been initiated within the Lewis program. This study is being done under contract NAS 3-13205 by the AiResearch Manufacturing Company. In this contract study, an analysis is being made to determine the effect on cooling performance of scaling down given turbine blade cooling configurations within fabrication constraints. Any attempt to determine the effect of chord size on cooling performance in a wide variety of engine applications would be prohibitively complex. As a consequence, for the analysis, simplifying assumptions were used. Some of the more important assumptions were (1) a fixed external aerodynamic shape, (2) constant solidity and constant corrected velocity triangles, (3) chords of 1.9, 2.54, and 3.81 centimeters (0.75, 1 and 1.5 in.), (4) a constant turbine span which was consistent with the radius ratio and aspect ratio for the 2.54-centimeter (1-in.) chord blade, (5) turbine inlet and cooling air inlet pressures and temperatures that would be expected in advanced engines, and (6) a creep life of 1000 hours for the blade material.

For a specific engine design when blade solidity is held constant, a reduction in chord length (i. e. , larger aspect ratio) will result in higher aerodynamic efficiency and a lighter weight turbine. However, fabrication limitations can make the cooling of short-chord blades difficult. Usually proportional reductions of the already small dimensions of the internal passages and wall thicknesses of the blades are not practical. Therefore, the ratio of internal to external heat transfer areas and the ratio of cooling airflow to gas flow areas decrease as chord size decreases. These factors can result in higher coolant flow requirements at a given turbine inlet temperature or in reduced allowable turbine inlet temperatures where cooling air pressure drop is a limitation.

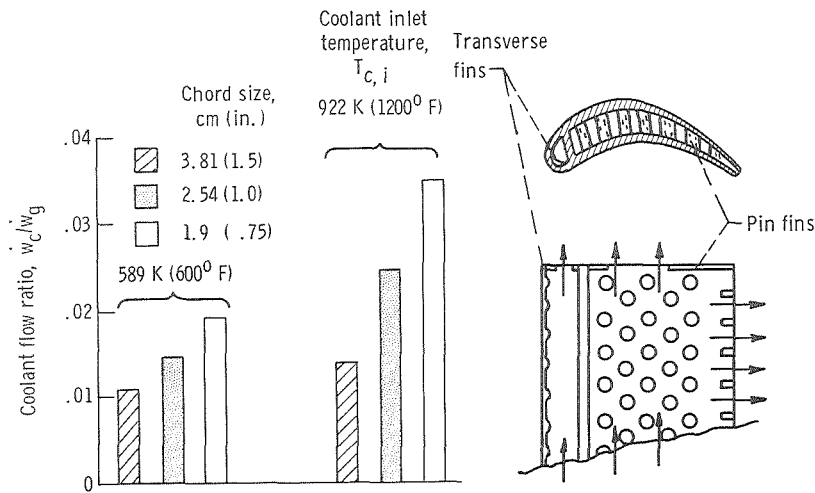


Figure 33. - Chord size as function of coolant required for convection-cooled blade. Effective gas temperature, 1422 K (2100° F); gas pressure, 103 newtons per square centimeter (150 psia).

The results of the analysis of one of the convection cooled blades considered in the study are shown in figure 33. The blade is of cast construction with transverse cast-in fins at the leading edge and cast-pin fins on a triangular spacing in the remainder of the blade. At the leading edge, airflows radially outward to exit at the tip. In the remainder of the blade, airflows both radially outward to exit at the tip and horizontally (chordwise) to exit through holes in the trailing edge. The results with this blade design are shown for a turbine inlet gas temperature of 1422 K (2100° F). This was the maximum allowable gas temperature for a 1000-hour life for the 1.9 centimeter (0.75 in.) chord blade. This figure shows an increased cooling flow requirement as chord size decreased. This trend held true for cooling air supply temperatures of both 589 and 922 K (600° and 1200° F). It can be concluded from this study that convection cooling of short-chord blades will be difficult. More investigations in the area are required.

The analytical study showed that for blades cooled by a combination of cooling methods, a consistent trend with chord size did not necessarily result. Some of the designs made use of film cooling in combination with convection cooling. Local thermal stresses induced by the film cooling resulted in the 1.9-centimeter (0.75-in.) and 2.54-centimeter (1-in.) chord blades having allowable temperatures higher than the 3.81-centimeter (1.5-in.) chord blade. Additional information on the effect of chord size on weight and cooling is contained in reference 64.

Fuel Cooling

The cooling discussions thus far presented in this paper have been limited to cooling

schemes using compressor bleed air as the coolant. As higher pressure ratios are used to improve the performance of engines for high speed aircraft, the corresponding rise in compressor bleed air temperature reduces the potential sink capacity of this coolant source. As a result, some method for reducing the compressor bleed air temperature or the use of some other coolant should be considered. Since fuel must of necessity be carried in the aircraft, attention has been given to the use of fuel to cool the hot parts of the engine before the fuel is burned in the engine combustor. Both ASTM Jet A and cryogenic fuels have been considered for turbine cooling purposes. The available heat sink in these fuels increases proportionally with the maximum allowable fuel temperature. However, the extent of fuel deposits in the fuel cooling passages may be a serious problem. The following discussion summarizes some of the results of fuel cooling studies to date.

A study into the possible use of commercially available ASTM Jet A fuel was made at Lewis and is reported in reference 65. This study was made using resistance-heated Nichrome V tubes to simulate fuel passages of an aircraft fuel to cooling air heat exchanger. The tube wall temperature was heated to 756 K (900° F) and the ASTM Jet A fuel temperature reached 644 K (700° F). After 20 hours of running, slight coking was observed in the tubes. The coking was not uniform, but was concentrated at local peaks. The peaks were found to be reduced when the oxygen content of the fuel was minimal.

This study is continuing under contract NAS 3-12432 with the Shell Development Company. Unpublished data obtained under this contract show operation for 100 hours with a fuel exit temperature of 811 K (1000° F) and a wall temperature of about 1006 K (1350° F). Coke deposits of only 0.00254-centimeter (0.001-in.) thickness were found in the 0.16-centimeter (1/16-in.) diameter tubes used.

Relative to the use of cryogenic fuels as coolants, a study on the thermal feasibility of using methane or hydrogen as coolants is reported in reference 66. This investigation involved a numerical heat-transfer analysis of methane- and hydrogen-cooled turbine vanes. Because of the large temperature difference between the coolant and the hot surface, an insulation barrier was required between the fuel cooling passages and the external vane surface to prevent adverse temperature gradients. Reference 66 also points out that an excessive fuel passage surface temperature could cause fuel cracking and/or carburization in methane cooling. The results of the calculations, made for a Mach 3 flight at an altitude of 22.8 kilometers (75 000 ft) indicated that the vane could be cooled with either methane or hydrogen for a local hot-spot gas temperature of 1639 K (2490° F) and that hydrogen would be slightly more effective as the coolant than methane. The reference also indicates that cooling a vane trailing edge with a cryogenic fuel will be very difficult if not impossible and suggests some alternate methods for cooling this region.

A summary of NASA research on cryogenic fuels for airbreathing gas turbine engines is given in reference 67. Problems requiring solutions before the use of cryogenic fuels

becomes feasible and areas requiring further research are noted in this reference. Some of the benefits from the heat sinks provided by ASTM Jet A fuels and methane fuels are presented in reference 68.

Predicted Metal Temperatures

The ability to accurately predict metal temperatures is essential for the design of reliable vanes and blades for use in advanced engines. Some of the correlations presented for both impingement and film cooling will be used in the following discussion. The predicted metal temperatures will also be compared with the measured temperatures for the vane shown in figure 4.

A knowledge of the flow distribution through the internal vane cooling passages must be known before vane metal temperatures can be predicted. In order to determine this flow distribution, a one-dimensional compressible flow network was used to simulate the vane cooling passages. Flow data obtained for the vane from tests run in the flow facility were used in this flow network; inlet and exit losses, friction pressure drops, and the coefficients for the one-dimensional flow network were determined. The resulting flow coefficients were then used in the flow analysis part of a combined flow and heat-transfer program to determine the flow distribution through the vane when it was tested in the cascade. For this latter purpose, the above mentioned flow coefficients, the known coolant inlet temperature, the external vane pressures known either from measurement or calculation, and the known total flow were held constant while the inlet pressure was analytically varied until the calculated total flow equalled the known total flow.

For the temperature calculations, distributions of the effective gas temperature and gas-to-blade heat-transfer coefficients are required. The velocity distribution is calculated from either the measured pressure distribution around the vane using isentropic perfect gas relationships or from one of several existing velocity prediction codes. Then, the effective gas temperature and gas-to-blade heat-transfer coefficients can be determined. The local effective gas temperature is calculated from

$$T_{ge} = T_{tot} - \frac{(1 - \Lambda)v_g^2}{2gJc_p} \quad (32)$$

where $\Lambda = Pr_f^{1/3}$ for turbulent flow or $\Lambda = Pr_f^{1/2}$ for laminar flow. For the vane leading edge,

$$h_g = 1.14 \operatorname{Re}_f^{0.05} \operatorname{Pr}_f^{0.4} \left[1 - \left| \frac{\theta}{90} \right|^3 \right] \frac{k_f}{D_{1e}} \quad (33)$$

where the characteristic dimension in the Reynolds number is the diameter of the leading edge cylinder, the property values are based on film temperature, and where θ ranges from -80° to 80° ; this is the equation for the gas-to-wall heat-transfer coefficient for flow over a cylinder. Equation (33) does not account for the effects of free stream turbulence on the heat-transfer coefficients over the vane leading edge region. This effect of turbulence on gas-to-blade heat-transfer coefficients is not yet fully known. However, equation (33) does yield approximate values which can be used to estimate vane temperatures over the vane leading edge region.

For the vane midchord region, the gas-to-vane heat-transfer was calculated by use of the turbulent flow flat plate correlation

$$h_g = 0.0296 \operatorname{Re}_f^{0.8} \operatorname{Pr}_f^{1/3} \frac{k_f}{x} \quad (34)$$

This correlation, like the one used for the leading edge region, is again only an approximation. Its use requires the assumption that turbulent flow exists along both vane surfaces. In reality, laminar flow might conceivably exist over a portion of a vane surface. However, the location of the point of transition is not yet well established and since the turbulent heat-transfer coefficient is larger than the laminar one, the use of equation (34) may yield higher vane temperatures than actually exist. Furthermore, the surfaces are not flat plates.

For the vane trailing edge region, where film cooling occurs, the film cooling effectiveness is calculated from (see ref. 69)

$$\eta_{\text{film}} = \frac{1}{1 + c_m \frac{x}{Ms}}$$

where c_m is the mixing coefficient indicating the level of turbulence. The values of η_{film} are then used to evaluate the adiabatic wall temperatures and this, in turn, is used with the convective heat-transfer coefficient h_g for the trailing edge region.

In order to complete the required heat balance and calculate vane temperatures, correlations for the internal heat-transfer coefficients must also be used. For impingement in the vane leading region, the correlation was taken from reference 55; for the vane

under consideration herein, this correlation reduced to

$$\bar{h}_{c,le} = 0.06549 Re_c^{0.7} \frac{k_c}{b} \quad (35)$$

where $Re_c = 4\dot{w}/\pi D$, \dot{w} is the impingement flow rate per jet, and D is the nozzle diameter. For the midchord region, the impingement correlation of reference 63 was used; it is

$$\bar{h}_{c,mc} = 0.286 Re_a^{0.625} \frac{k_c}{D} \quad (36)$$

where

$$Re_a = \frac{v_a c_n \rho}{\mu}$$

and

$$v_a = 6.63 v_n \frac{D}{z_n}$$

For the vane of figure 4, since $z_n/D < 6$, the potential core extends to the impingement surface and $v_a = v_n$. For the split trailing edge, a pin fin correlation

$$h_{c,te} = 0.248 Re_c^{0.594} Pr_c^{0.333} \frac{k_c}{d} \quad (37)$$

where $Re_c = \rho v_c d / \mu$ was used. This correlation is obtained from the Colburn factor.

After a nodal breakdown of the vane is made, enough information is now available to predict the vane temperatures. Iteration between the flow and heat-transfer portions of the calculation program must be made until the desired flow check results and the vane metal temperatures correspond to the assumed values required for evaluation of the gas-to-metal heat-transfer coefficients. Further details of metal temperature predictions are given in reference 70.

The preceding metal temperature prediction methods were applied to the vane of figure 4, and the results were compared with experimentally determined metal temperatures. It should be noted that these comparisons are for the purpose of illustrating the

prediction methods, and the correlations selected for use may not necessarily result in the best comparison between predictions and experiment over the complete vane. It should also be noted that, from the experiments, it was found that the inlet total gas temperature at the midspan vane leading edge region only differed from the effective gas temperature by about 25° R; this inlet total temperature was therefore used instead of the effective gas temperature for ease in calculation.

The predicted chordwise temperature distribution was determined for the midspan portion of the vane when operating in the static cascade (fig. 6) at the following conditions: $T_{Ti} = 839$ K (1050° F), $T_{c,i} = 304$ K (87° F), and $\dot{w}_c/\dot{w}_g = 0.053$. This predicted temperature distribution is shown as the dashed curve in figure 34. Experimental vane

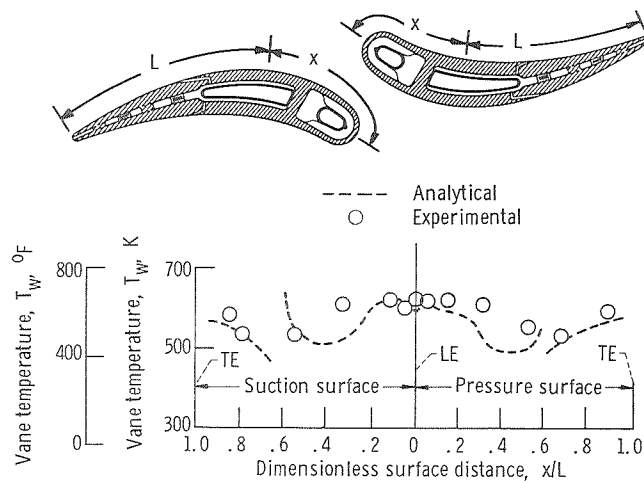


Figure 34. - Comparison of experimental and analytical vane temperatures for cascade tests. Turbine inlet temperature, 839 K (1050° F); coolant inlet temperature, 304 K (87° F); coolant flow ratio, 0.053.

temperature data for the same operating conditions in the static cascade are shown as the data points in figure 34. These data were obtained from measurements by thermocouples imbedded in the vane wall. Figure 34 shows good agreement between calculated and measured vane temperatures over most of the vane. The greatest divergence occurred in the midchord region, cooled by impingement.

A similar figure compares calculated and measured temperatures for the same vane under the following operating conditions in the engine (fig. 8): $T_{Ti} = 1506$ (2250° F), $T_{c,i} = 299$ K (78° F), and $\dot{w}_c/\dot{w}_g = 0.035$. The dashed curve of figure 35 shows this calculated distribution; measured data points are also shown for the same set of engine operating conditions. Although there were only half as many thermocouples on the engine vane as on the cascade vane, agreement between prediction and experiment was very

satisfactory. It should be noted that a more pronounced cusp at the vane leading edge is shown by the dashed line for the engine vane; unfortunately, the leading edge thermocouple did not function during the engine tests. Although the two figures show good agreement between predicted and measured vane temperatures, attempts to improve the prediction method are very much in order. In particular, for the midchord region, figure 35 shows that at the position just after the leading edge region, where there is little or no crossflow, the predicted temperatures are lower than the measured temperatures, and a correlation yielding a higher $h_{c,mc}$ than that of reference 63 should be used. Similarly, nearer the trailing edge where crossflow is considerably higher, the predicted temperature is too large.

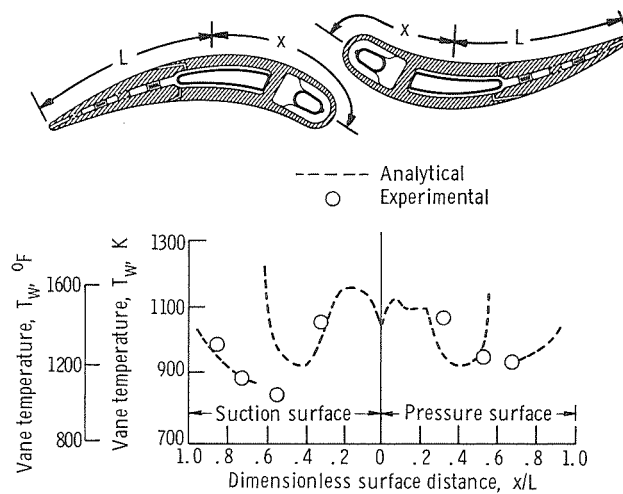


Figure 35. - Comparison of experimental and analytical vane temperatures for engine tests. Turbine inlet temperature, 1506 K (2250° F); coolant inlet temperature, 299 K (78° F); coolant flow ratio, 0.035.

Use of a computer code which includes boundary layer effects on heat-transfer should be considered. Research on the effect of turbulence and the location of the transition point from laminar to turbulent flow is very much in order. Improved impingement and film cooling correlations should be obtained. In other words, the method of predicting vane metal temperatures used herein should be altered as results from research in the areas noted above become available.

Vane temperatures calculated by the method described above are used as input to another computer program to determine vane or blade life. A description of this life calculation procedure is presented in references 71 and 72.

VANE AND BLADE FABRICATION AND STRUCTURAL PROBLEMS

FILM-CONVECTION COOLED VANE

Fabrication of vanes of this type (fig. 9(a)) on a production basis will be difficult. Prototype specimens for the experimental tests were made at Lewis. The convex and concave surfaces were made as separate halves from solid vane castings. The outer surface of each half was used as-cast and the inside finned surface and the film cooling holes were made by electrical discharge machining (EDM) on both halves. A separate piece made by EDM was used behind the leading edge to provide the impingement cooling hole array. Sheet metal baffles were brazed to the tops of the chordwise fins to form the coolant passages. The impingement piece was properly positioned between the two halves of the vane and the halves were joined by electron beam welding along the leading and trailing edges. This fabrication procedure was satisfactory for the short operating times required for research investigations. However, the joining technique used resulted in joints that had neither durability nor resistance to low cyclic fatigue.

To improve this type of vane or blade fabrication, a composite blade joining program was initiated. Two joining methods, gas pressure welding and activated diffusion brazing, are being investigated, under contracts NAS 3-10491 and NAS 3-12433 at Battelle Memorial Institute and the General Electric Company, respectively. The joining of materials such as TD Nickel Chromium and Udimet 700 to materials such as B1900 and René 80 are under investigation.

The joining processes are illustrated in figure 36. In gas pressure welding, the

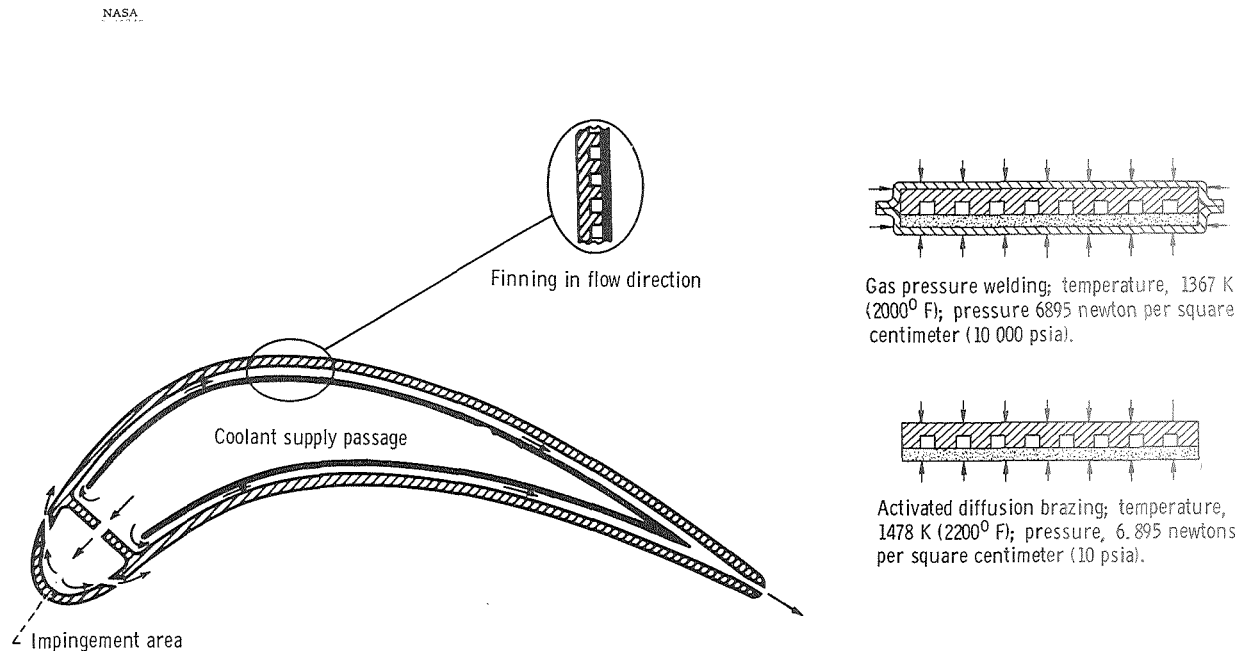


Figure 36. - Cooled blade fabrication.

parts to be joined are placed within an evacuated, lightweight container and then welded under high temperature and at a pressure on the order of 6895 newtons per square centimeter (10 000 psia) in an autoclave. However, the welding pressure is dependent on the configuration and materials to be joined. In activated diffusion brazing, a braze material is used whose composition closely matches that of, at least, one of the parent materials and includes a melting point depressant such as silicon. Brazing is done under a low pressure on the order of 6.895 newtons per square centimeter (10 psia) applied through contoured dies and at a temperature below the incipient melting point of the parent materials.

Shear test results at 1228 K (1750⁰ F) of gas pressure welded, Udimet 700-B1900, finned joining specimens are presented in figure 37. The experiment numbers refer to either different autoclave runs or lots of Udimet 700 materials. Each scatter band represents data from three specimens. The results demonstrate, generally, greater and more reproducible joint strengths with fins parallel to the load direction rather than with fins transverse to the load direction. Thermal cycling has a more deleterious effect on transverse fins than on fins parallel to the load.

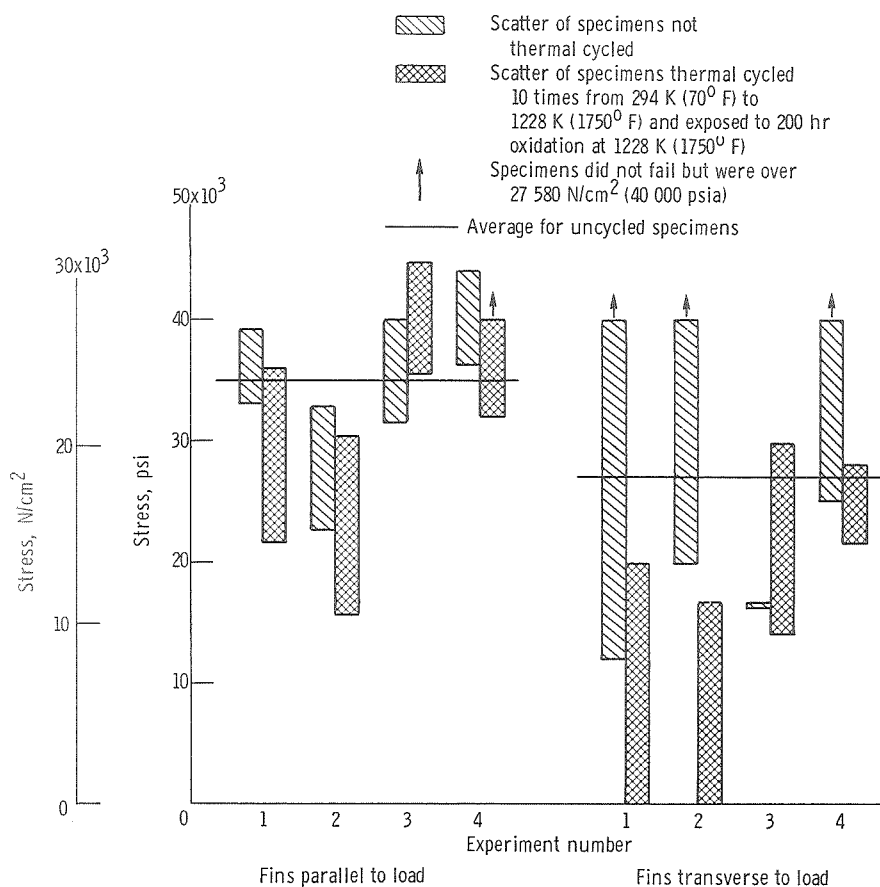


Figure 37. - Gas pressure welded flat Udimet 700-B1900 finned specimen joint shear strengths at 1228 K (1750⁰ F).

Stress rupture test results at 1228 K (1750° F) of activated diffusion brazed, Udimet 700-René 80, butt and finned lap joints are shown in figure 38 and reported in reference 14. For a 100-hour stress rupture life the butt joints demonstrate about 65 percent of the comparable Udimet 700 base material tensile strength. The butt joint data indicate that the stress rupture lives of the joints improved after 100 hours exposure to oxidation at 1228 K (1750° F) in an air atmosphere. The additional time at elevated temperature probably promoted further diffusion of silicon from the braze into the parent materials. Shear stress rupture strengths were only slightly lower than tensile stress rupture

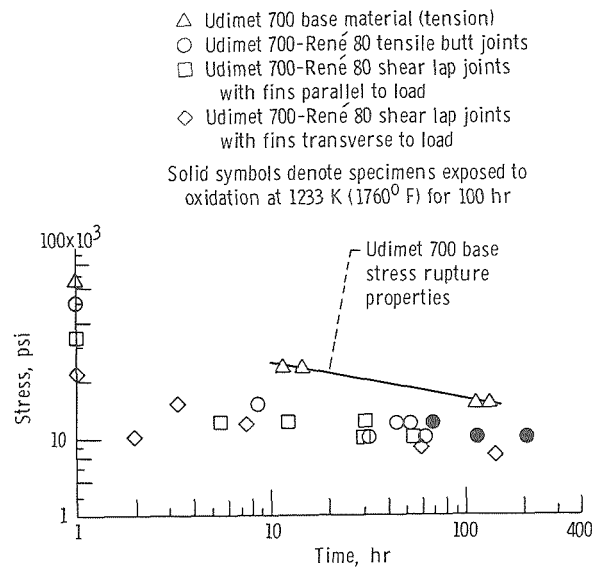


Figure 38. - Activated diffusion brazed Udimet 700-René 80 joint stress rupture strengths at 1228 K (1750° F).

strengths. The short-time Udimet 700-René 80 joint shear strengths shown on the extreme left of figure 38 are similar to the average short-time shear strengths shown in figure 37 for gas pressure welded joints. The joint strengths with both joining processes appear adequate for most rotor blade applications. As a final test of the activated diffusion brazing method, both TD NiCr and Udimet 700 finned shells were successfully brazed to the airfoils of René 80 production blades (see ref. 14).

FULL-COVERAGE FILM COOLED VANES

Laminated Sheet Metal Vane

The full-coverage film cooled vane, which was investigated under contract NAS

3-7913, is made of sheet metal laminates formed into an airfoil shell. This type of structure is feasible for a vane since excellent sheet materials, such as TD nickel chromium, are suitable for vanes. However, sheet metal construction imposes a temperature penalty on rotor blades for advanced airbreathing engines because the best sheet materials are inferior in high temperature strength capability to the better cast materials for the centrifugal stress levels that rotor blades would have to withstand.

Another potential problem that may be encountered with this type of vane is a cyclic ballooning of the entire airfoil during cyclic testing. Initially, in cascade tests at static conditions, airfoil ballooning was found to be a problem. This was solved by stiffening the inside of the shell with more laminates. However, there can still be enough movement of the pressure and suction sides under cyclic operation to cause longitudinal fatigue cracks at the leading edge in a relatively short time. It remains to be seen whether this problem can be solved by further stiffening of the vane.

Laminated Platelet Vane

This laminated configuration which was investigated under contract NAS 3-10495, is also fabricated from sheet metal and, therefore, has the same material property limitations with regard to rotor blades as the laminated sheet metal vane. However, this configuration presents an opportunity to tailor the coolant passage dimensions to the specific coolant requirements of the vane.

The laminated platelet vane was fabricated with laminates stacked in the spanwise direction. These laminates were all of the same contour and, therefore, were relatively cheap to photoetch; whereas radial platelets, each with a different contour would be considerably more expensive to photoetch. Tensile tests at 1255 K (1800⁰ F) of specimens cut from excess material around the vanes showed joint strengths to be equal to the material transverse strength. However, radial platelets are structurally necessary for rotor blades since a weak bond on a laminate will not cause a catastrophic failure as it would with platelets stacked in the spanwise direction. Another reason for the superiority of radial platelets is that sheet materials are usually stronger in the longitudinal (radial) direction than in the short transverse direction. However, since radial platelets have not as yet been investigated, their real advantages or disadvantages cannot be fully assessed.

TRANSPIRATION COOLED VANE

The porous shell of the transpiration cooled vane is fabricated by winding wire over

a removable mandrel and putting the resultant porous material through rolling and sintering operations to give it structural integrity as described in reference 73. The pores of this wire-form material are in the range of 5 to 40 micrometers in diameter. Therefore, the porous shell can be considered an ideal transpiration cooling material.

The main problem in applying transpiration cooling to turbine blades or vanes has been the susceptibility of the porous materials to flow restriction because of oxidation. Once significant oxidation starts, the metal temperature rises and further accelerates the oxidation and flow restriction process. An obvious method for alleviating the oxidation problem is to increase the pore sizes. However, this involves a departure from ideal transpiration cooling and a possible reduction in cooling effectiveness.

The laminated sheet metal specimen shown in figure 14(b) is an example of a full coverage film cooled material with relatively large coolant passages (see fig. 9(c)). From figure 14(b) it is apparent that the laminated sheet metal material has fewer but larger openings than the wire-form material, although the minimum constrictions do not lie at the sheet surface. The minimum constrictions are from 3 to 20 times the sizes of those in the wire-form sheet.

The internal structures of these materials are described in reference 73 for the wire-form material and in reference 29 for the laminated material.

A comparison of the oxidation characteristics of wire-form and laminate-form porous sheets of the same permeabilities and fabricated from the same material (Hastelloy X) is reproduced from reference 1 in figure 39. After 600 hours exposure in air at 1256 K (1800° F) the laminated material still retained about 75 percent of its original flow, whereas the wire-form material showed complete flow obstruction in 350 hours at

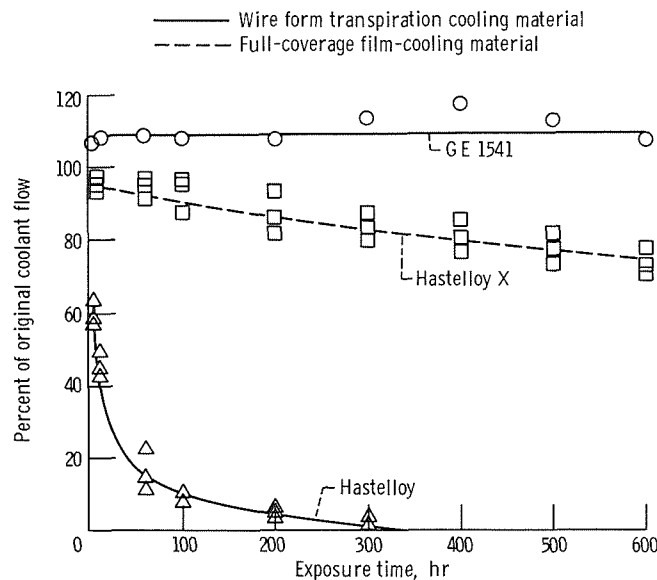


Figure 39. - Effect of oxidation on coolant flow.

1256 K (1800^o F). Flow data on wire-form specimens fabricated from GE 1541 (iron + chromium + aluminum + 1 percent yttrium) alloy after various oxidation exposures are also presented in figure 39. The GE 1541 material showed no flow reduction after 600 hours exposure at 1256 K (1800^o F) and represents a significant advance in the state-of-the-art of transpiration cooling at elevated temperatures.

The GE 1541 wire-form porous material was developed by the Filter Division of the Bendix Corporation under contract NAS 3-10477. The main fabrication problem involved sintering of the GE 1541 wires. The wires have an extremely adherent oxide which not only protects them against further oxidation but makes sintering very difficult. However, Bendix was able to develop a process for producing good sinter bonds in porous material made from GE 1541 wire. The main features of this process are (1) winding the wire over a stainless steel mandrel and then overwrapping it with molybdenum or tungsten wire, and (2) sintering the assembly in a vacuum furnace for 4 hours at 1478 K (2200^o F). Pressure is applied to the GE 1541 wires during sintering by the differential thermal expansion between the overwrap and the mandrel. A parting compound is used to prevent the GE 1541 from being bonded to the overwrap or the mandrel.

Under previous contracts Bendix screened 12 oxidation-resistant alloys for turbine blade transpiration cooling (ref. 74). On the basis of these tests, four alloys were chosen for further study in wire form (ref. 75). In reference 76 a method is presented for analytically determining the flow reduction from oxidation of wire-form sheets over a wide range of permeabilities using only oxidation data from wire specimens such as was obtained in reference 75.

BLADE LIFE RESEARCH

Turbine blade and vane life is acknowledged to be a function of the interaction between thermal fatigue, creep, and vibratory fatigue as well as oxidation and hot corrosion effects. With this in mind a facility was built that has the capability of being able to produce these phenomena individually and in combinations in cooled airfoil test specimens. This facility is the Hot Gas Facility for Turbine Blade Life Research.

A schematic of the facility is delineated in figure 40. The facility uses combustion air at pressures up to 113.7 newtons per square centimeter (150 psig) and at flow rates from 1.36 to 2.27 kilograms per second (3 to 5 lb/sec). The air enters the facility at ambient temperature and passes into the combustor assembly. The combustor assembly consists of a preburner and a main burner. In the preburner the temperature of the air is raised from ambient to 811 K (1000^o F). In the main burner additional heat is added raising the temperature to a preselected value between 1367 K (2000^o F) and 1922 K (3000^o F).

kilograms (30 000 lb) to the test specimen to simulate centrifugal forces in the turbine blade. In addition at a hold time or steady-state condition an alternating load of up to ± 4540 kilograms ($\pm 10\ 000$ lb) can be superimposed on the steady-state load to simulate a vibratory condition at frequencies from 25 to 60 hertz. The loading system is programmed to be synchronous with the temperature program allowing the combined systems to simulate a wide variety of engine conditions. Vitiated cooling air at temperatures up to 922 K (1200^o F) is provided to cool the test specimen. The flow rates in this system are between 0.136 to 0.318 kilogram per second (0.3 to 0.7 lb/sec). The facility is designed for automatic operation.

Continuous recording devices are provided to measure program variables and cycles applied. Provisions are incorporated to select a predetermined number of cycles for the test program and then shut down the system automatically once this has been attained.

The test specimen used in this facility is cast from the material to be investigated. The test specimen consist of a hollow airfoil, 10.16 centimeters (4 in.) long, with a chord of 5.08 centimeters (2 in.) and a nominal wall thickness of 0.152 centimeter (0.060 in.). Being hollow, the test specimen can be used with a variety of cooling configurations.

SUMMARY OF RESULTS

This report has provided an overall summary of NASA Lewis Research Center research on turbine cooling. Some of the more important conclusions and indications of the direction future research should take are as follows:

1. For a convection cooled turbine, reduction in cooling air temperature or increases in allowable metal temperature results in lower required coolant flow rates than can be obtained by improving convection efficiency of the configuration. Convection cooling becomes more difficult as chord size decreases.
2. At very high gas temperatures, film, impingement, and transpiration cooling may be required in any air-cooled configuration. Fuel cooling is a possible cooling method at these very high gas temperatures.
3. Improvements in fabrication techniques and improved material oxidation resistance can be a large benefit to the cooling methods required for very high gas temperature operation because of the complicated configurations involved and oxidation problems encountered in very small passages.
4. From similarity considerations, vane and blade temperatures determined experimentally for low values of gas and coolant temperatures can be scaled to estimate vane and blade temperatures for elevated values of gas and coolant temperatures.

5. Additional fundamental heat-transfer research is required in order to improve vane and blade temperature prediction methods. Boundary layer studies, turbulence effects, transition from laminar to turbulent flow, crossflow impingement and film cooling are some areas where further information would be useful.

6. Turbine life is influenced by many structural, cooling, and environmental factors. A program is being initiated on a turbine rig to evaluate the importance of these various factors and to develop life prediction methods applicable to air-cooled turbine vanes and blades.

Lewis Research Center,
National Aeronautics and Space Administration,
Cleveland, Ohio, June 10, 1971,
720-03.

APPENDIX-SYMBOLS

A	cross sectional area of flow passage
a	pin-fin transverse spacing to pin diameter ratio, S_t/d
B	$(\rho_c v_c c_{p,g})/h_{conv}$
b	slot width - impingement or jet half width
b'	distance from edge of boundary layer to edge of wall jet
C	constant
C_D	discharge coefficient
C_f	flow coefficient
c_n	center to center spacing
c_p	specific heat
D	diameter of flow passage or of film cooling hole or of impingement hole
D_h	hydraulic diameter
D_L	minimum flow hydraulic diameter (pin fin)
D_{le}	inside diameter of leading edge of vane or blade
d	pin fin diameter
$E_1, E_2, \left. \begin{array}{l} \\ \\ \end{array} \right\}$ $E_3, E_4 \left. \begin{array}{l} \\ \\ \end{array} \right\}$	determined from figs. 16, 17, and 14 of ref. 58 and from fig. 14 of ref. 60
f	friction factor
G	specific mass flow rate
G_S	mass flow rate per unit area through porous wall under standard conditions (upstream pressure, 17.0 N/cm^2 (24.7 psia); downstream pressure, 10.1 N/cm^2 (14.7 psia) at 294 K (70° F)
g	acceleration due to gravity
h	heat-transfer coefficient
J	mechanical equivalent of heat
k	thermal conductivity
L	length of vane suction or pressure surface
LE	leading edge

l	length of test surface from slot (film cooling) or length of test surface from stagnation point (impingement cooling)
M	film cooling blowing rate, $(\rho_c v_c)/(\rho_g v_g)$
Nu	Nusselt number
n	number of rows of pin fins
Pr	Prandtl number
p	pressure or exponent
q	heat flux or exponent
R	gas constant
Re	Reynolds number
S_t	transverse pin fin spacing
s	slot width-film cooling
T	temperature
TE	trailing edge
V	velocity in wall jet region
V_m	maximum velocity in wall jet region
v	velocity
\dot{w}	flow rate
x, y, z	orthogonal co-ordinates
z_n	distance between nozzle and impingement point
$z_{1/2}$	value of z for $V = 1/2 V_m$
α	viscous resistance coefficient
β	initial resistance coefficient
δ	boundary layer thickness
ξ	$(z - \delta)/b'$
$\xi_{1/2}$	$(z_{1/2} - \delta)/b'$
η'_{conv}	$(T_{c,o} - T_{c,i})/(T_{w,i} - T_{c,i})$
η'_{film}	$(T_{ge} - T_{aw})/(T_{ge} - T_{c,o})$
η'_{film}	$(T_{c,o} - T_{c,i})/(T_{w,o} - T_{c,i})$
η'_{trans}	$(T_{c,o} - T_{c,i})/(T_{w,o} - T_{c,i})$

θ	angular distance from stagnation point
θ^*	$(T_c - T_{ge}) / (T_w - T_{ge})$
Λ	recovery factor
λ	film cooling injection angle as measured from z axis in yz plane
μ	viscosity
ν	kinematic viscosity
ρ	density
τ	thickness
φ	temperature difference ratio
ψ	film cooling injection angle as measured from x axis in xy plane

Subscripts:

a	arrival velocity
aw	adiabatic wall
b	slot width
conv	convection
D_h	hydraulic diameter
d	pin fin diameter
f	based on film temperature
fr	friction
g	gas
ge	effective gas
i	in or inside
le	leading edge
max	maximum
mc	midchord
min	minimum
n	nozzle
o	out or outside
Ti	turbine inlet

Tot total
te trailing edge
trans transpiration
w wall
1 upstream
2 downstream

Superscript:

— average

REFERENCES

1. Esgar, Jack B. ; Colladay, Raymond S. ; and Kaufman, Albert: An Analysis of the Capabilities and Limitations of Turbine Air Cooling Methods. NASA TN D-5992, 1970.
2. Stepka, Francis S. : Considerations of Turbine Cooling Systems for Mach 3 Flight. NASA TN D-4491, 1968.
3. Goldstein, R. J. ; Eckert, E. R. G. ; and Ramsey, J. W. : Film Cooling with Injection Through a Circular Hole. Rep. HTL-TR-82, Minnesota Univ. (NASA CR-54604), May 14, 1968.
4. Metzger, D. E. ; Carper, H. J. ; and Swank, L. R. : Heat Transfer with Film Cooling Near Nontangential Injection Slots. J. Eng. Power, vol. 90, no. 2, Apr. 1968, pp. 157-163.
5. Metzger, D. E. ; and Fletcher, D. D. : Surface Heat Transfer Immediately Downstream of Flush, Non-Tangential Injection Holes and Slots. Paper 69-523, AIAA, June 1969.
6. Goldstein, R. J. ; Eckert, E. R. G. ; Eriksen, V. L. ; and Ramsey, J. W. : Film Cooling Following Injection Through Inclined Circular Tubes. Rep. HTL-TR-91, Minnesota Univ. (NASA CR-72612), Nov. 1969.
7. Moffat, R. J. ; and Kays, W. M. : The Turbulent Boundary Layer on a Porous Plate: Experimental Heat Transfer with Uniform Blowing and Suction. Rep. HMT-1, Stanford Univ. , Aug. 1967.
8. Simpson, R. L. ; Kays, W. M. ; and Moffat, R. J. : The Turbulent Boundary Layer on a Porous Plate: An Experimental Study of the Fluid Dynamics with Injection and Suction. Rep. HMT-2, Stanford Univ. , Dec. 1967.
9. Whitten, D. G. ; Kays, W. H. ; and Moffat, R. J. : The Turbulent Boundary Layer on a Porous Plate: Experimental Heat Transfer with Variable Suction, Blowing, and Surface Temperature. Rep. HMT-3, Stanford Univ. , Dec. 1967.
10. Julien, H. L. ; Kays, W. M. ; and Moffat, R. J. : The Turbulent Boundary Layer on a Porous Plate: An Experimental Study of the Effects of a Favorable Pressure Gradient. Rep. HMT-4, Stanford Univ. (NASA CR-104140), Apr. 1969.
11. Thielbahr, W. H. ; Kays, W. M. ; and Moffat, R. J. : The Turbulent Boundary Layer on a Porous Plate: Experimental Heat Transfer with Blowing, Suction, and Favorable Pressure Gradient. Rep. HMT-5, Stanford Univ. (NASA CR-104141), Apr. 1969.

12. Hrycak, Peter; Lee, David T.; Gauntner, James W.; and Livingood, John N. B.: Experimental Flow Characteristics of a Single Turbulent Jet Impinging on a Flat Plate. NASA TN D-5690, 1970.
13. Gauntner, James W.; Livingood, John N. B.; and Hrycak, Peter: Survey of Literature on Flow Characteristics of a Single Turbulent Jet Impinging on a Flat Plate. NASA TN D-5652, 1970.
14. Kaufman, A.; Berry, T. F.; and Meiners, K. E.: Joining Techniques for Fabrication of Composite Air-Cooled Turbine Blades and Vanes. Presented at the ASME Gas Turbine Conference and Product Show, Houston, Texas, Mar. 28-Apr. 1, 1971.
15. Ellerbrock, Herman H.; and Cochran, Reeves P.: Turbine Cooling Research. Aircraft Propulsion. NASA SP-259, 1971, pp. 57-96.
16. Clark, John S.; Richards, Hadley T.; Poferl, David J.; and Livingood, John N. B.: Coolant Pressure and Flow Distribution Through an Air-Cooled Vane for a High-Temperature Gas Turbine. NASA TM X-2028, 1970.
17. Calvert, Howard F.; Cochran, Reeves P.; Dengler, Robert P.; Hickel, Robert O.; and Norris, James W.: Turbine Cooling Research Facility. NASA TM X-1927, 1970.
18. Pollack, Frank G.; and Hickel, Robert O.: Surface Temperature Mapping with Infrared Photographic Pyrometry for Turbine Cooling Investigations. NASA TN D-5179, 1969.
19. Gladden, Herbert J.; Dengler, Robert P.; Evans, David G.; and Hippensteele, Steven A.: Aerodynamic Investigation of Four-Vane Cascade Designed for Turbine Cooling Studies. NASA TM X-1954, 1970.
20. Whitney, Warren J.: Comparative Study of Mixed- and Isolated-Flow Methods for Cooled-Turbine-Performance Analysis. NASA TM X-1572, 1968.
21. Whitney, Warren J.: Analytical Investigation of the Effect of Cooling Air on Two-Stage Turbine Performance. NASA TM X-1728, 1969.
22. Whitney, Warren J.; Szanca, Edward M.; and Behning, Frank P.: Cold-Air Investigation of a Turbine with Stator-Blade Trailing-Edge Coolant Ejection. I - Overall Stator Performance. NASA TM X-1901, 1969.
23. Prust, Herman W., Jr.; Behning, Frank P.; and Bider, Bernard: Cold-Air Investigation of a Turbine with Stator-Blade Trailing-Edge Coolant Ejection. II - Detailed Stator Performance. NASA TM X-1963, 1970.

24. Szanca, Edward M. ; Schum, Harold J. ; and Prust, Herman W. , Jr. : Cold-Air Investigation of a Turbine with Stator-Blade Trailing-Edge Coolant Ejection. III - Overall Stage Performance. NASA TM X-1974, 1970.
25. Yeh, Frederick C. ; and Cochran, Reeves P. : Comparison of Experimental and Ideal Leakage Flows Through Labyrinth Seals for Very Small Pressure Differences. NASA TN X-1958, 1970.
26. Yeh, Frederick C. ; Poferl, David J. ; Cochran, Reeves P. ; and Richards, Hadley T. : Cooling Airflow Through a Stationary Turbine Disk and Blade. NASA TM X-2171, 1971.
27. Lesco, Daniel J. ; Sturman, John C. ; and Nieberding, William C. : Rotating Shaft-Mounted Microelectronic Data System. NASA TN D-5678, 1970.
28. Anderson, R. D. ; and Nealy, D. A. : Evaluation of Laminated Porous Material for High-Temperature Air-Cooled Turbine Blades. Rep. EDR-4968, General Motors Corp. (NASA CR-72281), Jan. 16, 1967.
29. Nealy, D. A. ; Anderson, R. D. ; and Hufford, A. A. : Design and Experimental Evaluation of a Turbine Vane Fabricated from Laminated Porous Material. Rep. EDR-6296, General Motors Corp. (NASA CR-72649), July 31, 1969.
30. Klessig, C. E. : Investigation of Laminated Convection-Film Cooled Turbine Stator Vanes. Rep. AGC-2100-1, Aerojet Liquid Rocket Co. (NASA CR-72506), July 31, 1970.
31. Lombardo, S. ; Moskowitz, S. L. ; and Schnure, S. A. : Experimental Results of a Transpiration-Cooled Turbine Operated in an Engine for 150 Hours at 2500° F Turbine Inlet Temperature. Paper 67-GT-29, ASME, Mar. 1967.
32. Moskowitz, S. L. ; and Schober, T. E. : Design and Test of a Small Turbine at 2500° F with Transpiration Cooled Blading. Paper 690035, SAE, Jan. 1969.
33. Mindrala, Joseph ; Wysocki, Dennis A. ; and Hollenbeck, Brian L. : J65-W-18 Engine Evaluation of Curtiss-Wright Transpiration-Cooled Turbine Blades and Variable-Geometry Turbine Concepts. Rep. NAPTC-ATD-129, Naval Air Propulsion Test Center, Nov. 1967.
34. Kays, W. M. ; and London, A. L. : Compact Heat Exchangers. Second ed. , McGraw-Hill Book Co. , Inc. , 1964, p. 184.
35. Rohde, John E. ; Richards, Hadley T. ; and Metger, George W. : Discharge Coefficients for Thick Plate Orifices with Approach Flow Perpendicular and Inclined to the Orifice Axis. NASA TN D-5467, 1969.

36. Glauert, M. B.: The Wall Jet. *J. Fluid Mech.*, vol. 1, pt. 6, Dec. 1956, pp. 625-643.
37. Abramovich, Genrikh N.: *The Theory of Turbulent Jets*. M.I.T. Press, 1963.
38. Kaufman, Albert; and Richards, Hadley, T.: Investigation of Flow Characteristics of Some Wire-Form and Laminate-Form Porous Materials. NASA TM X-2111, 1970.
39. Gladden, Herbert J.; Hippensteele, Steven A.; Hickel, Robert O.; and Dengler, Robert P.: Radiation Heat Transfer Characteristics of Turbine Vane Airfoils in a Water-Cooled Cascade. NASA TM X-2203, 1971.
40. Moffitt, Thomas P.; Nosek, Stanley M.; and Roelke, Richard J.: Turbine Aerodynamic Considerations for Advanced Turbines. Aircraft Propulsion. NASA SP-259, 1971, pp. 37-55.
41. Ramsey, J. W.; and Goldstein, R. J.: Interaction of a Heated Jet with a Deflecting Stream. Rep. HTL-TR-92, Minnesota Univ. (NASA CR-72613), Apr. 1970.
42. Wieghardt, K.: Hot-Air Discharge for De-Icing. Trans. No. F-TS-919-Re, Army Air Forces, Air Material Command, Dec. 1946.
43. Burggraf, F.; Murtaugh, J. P.; and Wilton, M. E.: Design and Analysis of Cooled Turbine Blades. Part I - Leading and Trailing Edge Configurations. Rep. R68AEG101, General Electric Co. (NASA CR-54513), Jan. 1, 1968.
44. Burggraf, F.; Murtaugh, J. P.; and Wilton, M. E.: Design and Analysis of Cooled Turbine Blades. Part II - Convection Cooled Nozzles and Buckets. Rep. R68AEG102, General Electric Co. (NASA CR-54514), Jan. 1, 1968.
45. Burggraf, F.; Murtaugh, J. P.; and Wilton, M. E.: Design and Analysis of Cooled Turbine Blades. Part III - Transpiration and Multiple Small Hole Film Cooled Nozzle and Buckets. Rep. R68AEG103, General Electric Co. (NASA CR-54515), Jan. 1, 1968.
46. Burggraf, F.; Murtaugh, J. P.; and Wilton, M. E.: Design and Analysis of Cooled Turbine Blades. Part IV - Combined Methods of Cooling. Rep. R68AEG104, General Electric Co. (NASA CR-54512), Jan. 1, 1968.
47. Danforth, C. E.; and Burggraf, F.: Design and Analysis of Cooled Turbine Blades. Part V - Life Prediction of Selected Designs. Rep. R68AEG105, General Electric Co. (NASA CR-72412), Aug. 1968.
48. Mickley, H. S.; Ross, R. C.; Squyers, A. L.; and Stewart, W. E.: Heat, Mass, and Momentum Transfer for Flow Over a Flat Plate with Blowing or Suction. NACA TN 3208, 1954.

49. Clevenger, W. ; and Tabakoff, W. : Investigation of the Heat Transfer Characteristics of a Two-Dimensional Jet Impinging on a Semi-Cylinder. Rep. THEMIS-AE-69-5, Univ. of Cincinnati (AROD-T-4-10-E, DDC No. AD-697165), Oct. 1969.
50. Dyban, E. P. ; and Mazur, A. I. : Heat Transfer During Injection of a Plane Air Jet Into a Concave Surface. *Inzhenerno-Fiz. Zh.* , vol. 17, Nov. 1969, pp. 785-790.
51. Jusionis, Vytautas J. : Heat Transfer from Impinging Gas Jets on an Enclosed Concave Surface. *J. Aircraft*, vol. 7, no. 1, Jan. - Feb. 1970, pp. 87-88.
52. Burggraf, F. : Average Heat Transfer Coefficients with a Row of Air Jets Discharging Into a Half Cylinder. M. S. Thesis, Univ. Cincinnati, 1967.
53. Metzger, D. E. ; Yamashita, T. ; and Jenkins, C. W. : Impingement Cooling of Concave Surfaces with Lines of Circular Air Jets. Paper 68-WA/GT-1, ASME, Dec. 1968.
54. Jenkins, C. W. ; and Metzger, D. E. : Local Heat Transfer Characteristics of Concave Cylindrical Surfaces Cooled by Impinging Slot Jets and Lines of Circular Jets with Spacing Ratios 1.25 to 6.67. Rep. ME-694, Arizona State Univ. , May 1969.
55. Chupp, Raymond E. ; Helms, Harold E. ; McFadden, Peter W. ; and Brown, T. R. : Evaluation of Internal Heat-Transfer Coefficients for Impingement-Cooled Turbine Airfoils. *J. Aircraft*, vol. 6, no. 3, May-June 1969, pp. 203-208.
56. Schuh, H. ; and Pettersson, R. : Heat Transfer by Arrays of Two-Dimensional Jets Directed Normal to Surfaces Including the Effects of a Superposed Wall-Parallel Flow. Proceedings of Third International Heat Transfer Conference. Vol. 2, AIChE, 1966, pp. 280-291.
57. Kercher, D. M. ; and Tabakoff, W. : Heat Transfer by a Square Array of Round Air Jets Impinging Perpendicular to a Flat Surface Including the Effect of Spent Air. *J. Eng. Power*, vol. 92, no. 1, Jan. 1970, pp. 73-82.
58. Kercher, D. M. : Heat Transfer by a Multiple Array of Round Jets Impinging Perpendicular to a Flat Surface Including Effects of Spent Air. M. S. Thesis, Univ. Cincinnati, 1967.
59. Huang, G. C. : Investigations of Heat-Transfer Coefficients for Air Flow Through Round Jets Impinging Normal to a Heat-Transfer Surface. *J. Heat Transfer*, vol. 85, no. 3, Aug. 1963, pp. 237-245.
60. Freidman, S. J. ; and Mueller, A. C. : Heat Transfer to Flat Surfaces. Proceedings of the General Discussion on Heat Transfer. *Inst. Mech. Eng.* , 1951, pp. 138-142.

61. Hilgeroth, E. : Heat Transfer in Jet Flow Perpendicular to the Transfer Surface. Chem. Ing. Tech. , vol. 37, no. 12, 1965, pp. 1264-1272.
62. Ott, Hanns H. : Heat Transfer to a Plate Cooled by Air Flow. Schweiz. Bauzeitung, vol. 79, no. 46, Nov. 16, 1961.
63. Gardon, Robert; and Cobonpue, John: Heat Transfer Between a Flat Plate and Jets of Air Impinging on It. International Developments in Heat Transfer. ASME, 1963, pp. 454-460.
64. Esgar, Jack B. ; Schum, Eugene F. ; and Curren, Arthur N. : Effect of Chord Size on Weight and Cooling Characteristics of Air-Cooled Turbine Blades. NACA TR 1345, 1958.
65. Watt, James J. ; Evans, Albert Jr. ; and Hibbard, Robert R. : Fouling Characteristics of ASTM Jet A Fuel When Heated to 700^o F in a Simulated Heat Exchanger Tube. NASA TN D-4958, 1968.
66. Colladay, Raymond S. : Thermal Feasibility of Using Methane or Hydrogen Fuel for Direct Cooling of a First-Stage Turbine Stator. NASA TN D-6042, 1970.
67. Esgar, Jack B. : Cryogenic Fuels for Aircraft. Aircraft Propulsion. NASA SP-259, 1971, pp. 397-420.
68. Evans, David G. ; Furgalus, Keith A. ; and Stepka, Francis S. : Turbine Aerodynamic and Cooling Requirements for a Turbojet Powered Mach 3 Transport Using Methane Fuel. NASA TN D-5928, 1970.
69. Juhasz, A. J. ; and Marek, C. J. : Combustor Liner Film Cooling in the Presence of High Free-Stream Turbulence. NASA TN D-6360, 1971.
70. Gladden, Herbert J. ; Gauntner, Daniel J. ; and Livingood, John N. B. : Analysis of Heat-Transfer Tests of an Impingement, Convection, Film Cooled Vane in a Cascade. NASA TM X-2376, 1971.
71. Kaufman, Albert: Steady-State Stress Relaxation Analysis of Turbine Blade Cooling Designs. NASA TN D-5282, 1969.
72. Kaufman, Albert: Analytical Study of Cooled Turbine Blades Considering Combined Steady-State and Transient Conditions. NASA TM X-1951, 1970.
73. Wheeler, H. L. , Jr. : Transpiration Cooling in the High Temperature Gas Turbine. Bendix Filter Div. , Bendix Corp. , Mar. 1964.
74. Cole, Fred W. ; Padden, James B. ; and Spencer, Andrew R. : Oxidation Resistant Materials for Transpiration Cooled Gas Turbine Blades. I. Sheet Specimen Screening Tests. NASA CR-930, 1968.

75. Cole, Fred W. ; Padden, James B. ; and Spencer, Andrew R. : Oxidation Resistant Materials for Transpiration Cooled Gas Turbine Blades. II. Wire Specimen Tests. NASA CR-1184, 1968.
76. Kaufman, Albert: Analytical Study of Flow Reduction Due to Oxidation of Wire-Form Porous Sheet for Transpiration Cooled Turbine Blades. NASA TN D-5001, 1969.



POSTMASTER: If Undeliverable (Section 158
Postal Manual) Do Not Return

"The aeronautical and space activities of the United States shall be conducted so as to contribute . . . to the expansion of human knowledge of phenomena in the atmosphere and space. The Administration shall provide for the widest practicable and appropriate dissemination of information concerning its activities and the results thereof."

— NATIONAL AERONAUTICS AND SPACE ACT OF 1958

NASA SCIENTIFIC AND TECHNICAL PUBLICATIONS

TECHNICAL REPORTS: Scientific and technical information considered important, complete, and a lasting contribution to existing knowledge.

TECHNICAL NOTES: Information less broad in scope but nevertheless of importance as a contribution to existing knowledge.

TECHNICAL MEMORANDUMS: Information receiving limited distribution because of preliminary data, security classification, or other reasons.

CONTRACTOR REPORTS: Scientific and technical information generated under a NASA contract or grant and considered an important contribution to existing knowledge.

TECHNICAL TRANSLATIONS: Information published in a foreign language considered to merit NASA distribution in English.

SPECIAL PUBLICATIONS: Information derived from or of value to NASA activities. Publications include conference proceedings, monographs, data compilations, handbooks, sourcebooks, and special bibliographies.

TECHNOLOGY UTILIZATION PUBLICATIONS: Information on technology used by NASA that may be of particular interest in commercial and other non-aerospace applications. Publications include Tech Briefs, Technology Utilization Reports and Technology Surveys.

Details on the availability of these publications may be obtained from:

**SCIENTIFIC AND TECHNICAL INFORMATION OFFICE
NATIONAL AERONAUTICS AND SPACE ADMINISTRATION
Washington, D.C. 20546**